

**BSc thesis in Applied Earth Sciences for the  
department Geoscience and Engineering**

**Micro-scale effects of stylolite orientation on  
the motion of tensile failure: A study analyzing  
strain fields of stylolite limestones using  
Particle Image Velocimetry**

**Barry Versluis  
2020**





MICRO-SCALE EFFECTS OF STYLOLITE ORIENTATION ON THE  
MOTION OF TENSILE FAILURE: A STUDY ANALYZING STRAIN  
FIELDS OF STYLOLITE LIMESTONES USING PARTICLE IMAGE  
VELOCIMETRY

A thesis submitted to the Delft University of Technology in partial fulfillment  
of the requirements for the degree of

Bachelor of Science in Applied Earth Sciences

by

Barry Versluis

Juli 2020

An electronic version of this thesis is available at <http://repository.tudelft.nl/>.

Barry Versluis: *Micro-scale effects of stylolite orientation on the motion of tensile failure: A study analyzing strain fields of stylolite limestones using Particle Image Velocimetry* (2020)

The work in this thesis was made for the:

Section of Applied Geophysics & Petrophysics  
Department of Geoscience & Engineering  
Faculty of Civil Engineering & Geosciences  
Delft University of Technology

Supervisor:

Dr. A. Pluymakers, TU Delft

Thesis committee:

Dr. A. Barnhoorn, TU Delft  
Dr. A. Pluymakers, TU Delft

## ABSTRACT

Many laboratory tests of samples where the rock fractures are based on meso-scale (cm) characterization of effective 'intact' strength parameters neglecting the microstructure effects. Understanding fracturing processes at micro-scale (mm) will require models with microstructure data. However, data is lacking on micro-scale.

Stylolites are natural rock-rock interlocked interfaces which form by a localized dissolution process and their interface contains minerals and material different from that in the surrounding host rock. Microstructures such as stylolites influence the tensile stress behaviour in a rock formation. We are interested in stylolites because they can act as drains or as barriers to flow. Therefore, we introduce a study where we investigate on micro-scale failure mechanisms of limestone samples with stylolites in diverse orientations.

In preceding study (Pluymakers et al., pers. comm.) a series of Brazilian Disc Tests was performed on eleven samples all including stylolites of micro-scale carbonate samples from the "Treuchtlinger Marmor" formation from the Molasse Basin (Munich, Germany). All experiments were filmed using a DSLR camera.

In this study we aim to develop the use of the Particle Image Velocimetry method to analyze such type of movies. We use the developed Particle Image Velocimetry method to analyze three of the movies of the preceding study, which contained samples where the stylolite is at different angles to the horizontal axis of the sample, so to  $\sigma_3$ . Two samples has an angle of  $90^\circ$  between the stylolite and  $\sigma_3$  and one with an angle of  $40^\circ$ .

In this open-source software the pixel displacement is analyzed in frames (i.e. consecutive images, 'before' and 'after' image) and it calculates the velocity distribution within the framepairs, but it is also used to derive, display and export multiple parameters of the flow pattern. In this study we derived and displayed the strain rate on the image pairs.

The results show that the strain field of the two limestone samples of a  $90^\circ$  stylolite behaves identical in the two major stress drops (i.e.  $\Delta Stress$ ) from the stress-displacement curve. However, the sample with a stylolite of  $40^\circ$  behaves differently. For the two  $90^\circ$  oriented stylolites random extension and compression takes place at the first highest negative stress drop and symmetric extension takes place at the second highest negative stress drop from the stress-displacement curve. However, for the  $40^\circ$  oriented stylolites asymmetric extension takes place at the first highest negative stress drop from the stress-displacement curve. And random extension at the second drop. Another result of this study is that the strain rate obtained from PIVlab, the strain rate per stress drop (MPa) (i.e. in the stress displacement-curve) in both the two  $90^\circ$  stylolite samples and the  $40^\circ$  sample were different.

To put this work in the broader context of the energy transition, we consider the rapid development of the geothermal sector. Nowadays geothermal energy is considered as one of many alternative sources of energy using

the hot water in the Earth's surface to generate electricity and power heating/cooling systems. The Dinantian carbonates in the Netherlands and the "Treuchtlinger Marmor" carbonates from Germany are of interest for Ultra Deep Geothermal wells, because of their high geothermal potential. To enhance the porosity/permeability in a formation where hot water needs to be extracted hydraulic fracturing can be an option and this study gives insight about how the rock formations on micro-scale behave when tensile failure occurs. Tensile is one of the most important properties to be evaluated for any textile material (i.e. rocks). Tensile failure is important because it occurs when the stress on a component exceeds the strength of the material thus it determines the strength of a rock and consequently is influenced by single plane of weakness such as stylolites.

## ACKNOWLEDGEMENTS

Thanks to everyone, especially to Dr. A. Pluymakers for her time and positive attitude guiding me through my Bachelor End Project. Also thanks to Dr. A. Barnhoorn, my family, friends and my girlfriend.

My special thanks go to my parents for their support during my Bachelor. I am grateful that my lovely girlfriend was always there for me. I am also very grateful for the opportunities which the TU Delft provided to develop myself as a person and as a future engineer. It means the 'Earth' to me.

It was a great honour to study at the Delft University of Technology and now it is time for a next step in my career.

Barry Versluis



# CONTENTS

Abstract	v
List of Figures	xi
List of Tables	xiii
List of Algorithms	xv
Acronyms	xvii
1 INTRODUCTION	1
2 STYLOLITE TYPES AND CHARACTERISTICS	5
3 PETROPHYSICAL PROPERTIES OF THE "TREUCHTLINGER MARMOR"	7
4 MATERIAL STUDIED AND EXPERIMENTAL SET-UP	9
4.1 Material origin and preparation of the samples . . . . .	9
4.2 Experimental procedure . . . . .	10
4.2.1 Procedure and results of preceding study . . . . .	10
4.2.2 Procedure of this study . . . . .	11
5 MOVIE PROCESSING AND PIV MODELLING	15
5.1 Movie processing . . . . .	15
5.2 Particle Image Velocimetry modelling . . . . .	18
5.2.1 Background theory of the PIVlab tool . . . . .	18
5.2.2 Procedure PIVlab . . . . .	19
6 RESULTS AND ANALYSIS FROM DATA-SET	23
6.1 Results of scenario a) 10 frames and b) 50 frames . . . . .	23
6.2 Results of scenario c) specific frames . . . . .	24
6.2.1 Results for a 90 degree stylolite (TM236) . . . . .	25
6.2.2 Results for a 90 degree stylolite (TM241) . . . . .	28
6.2.3 Results for a 40 degree stylolite (TM313) . . . . .	32
7 DISCUSSION	37
7.1 Limitation of PIV-method . . . . .	37
7.2 Explanation results . . . . .	38
7.3 Wider perspective of the study into the field of Applied Earth Sciences . . . . .	39
7.3.1 Societal relevance . . . . .	39
7.3.2 Scientific relevance . . . . .	39
7.3.3 Environmental relevance . . . . .	40
7.3.4 BSc-curriculum . . . . .	41
7.4 Recommendation . . . . .	42
8 CONCLUSION	43
Bibliography	44
A TM236	47
B TM241	53
C TM313	57
D TIMETABLE	61



## LIST OF FIGURES

Figure 1.1	Stylolite . . . . .	1
Figure 1.2	Four configurations Brazilian Disc Test . . . . .	2
Figure 1.3	Brazilian Disc Test . . . . .	3
Figure 2.1	Diagram of calculating stylolite sealing capacity . . . . .	5
Figure 4.1	Treuchtlinger Marmor . . . . .	9
Figure 4.2	Stratigraphy Malm . . . . .	10
Figure 4.3	Treuchtlinger Marmor discs with orientation of stylolites . . . . .	11
Figure 4.4	Treuchtlinger Marmor discs with stress displacement curve of samples . . . . .	12
Figure 5.1	Cropped Frame 2900 and 6190 for TM241 . . . . .	17
Figure 5.2	Frame 5136 5801 . . . . .	18
Figure 5.3	Stress Displacement curves TM236 and TM241 . . . . .	20
Figure 5.4	Stress Displacement curves TM313 . . . . .	21
Figure 5.5	PIVlab result . . . . .	22
Figure 6.1	PIVlab result every 10 frames TM236 . . . . .	23
Figure 6.2	PIVlab result every 50 frames TM241 . . . . .	24
Figure 6.3	TM236: Frame 4180-4280 . . . . .	25
Figure 6.4	TM236: Frame 4720-6030 . . . . .	26
Figure 6.5	TM236: Frame 4280-4480 . . . . .	26
Figure 6.6	Stress Displacement curves TM236 . . . . .	28
Figure 6.7	TM241: Frame 2900-3084 . . . . .	29
Figure 6.8	TM241: Frame 5857-6079 . . . . .	29
Figure 6.9	TM241: Frame 4859-5136 . . . . .	30
Figure 6.10	Stress Displacement curves TM241 . . . . .	32
Figure 6.11	TM313: Frame 3106-3119 . . . . .	33
Figure 6.12	TM313: Frame 3823-3898 . . . . .	33
Figure 6.13	TM313: Frame 4013-4084 . . . . .	34
Figure 6.14	Stress Displacement curves TM313 . . . . .	36
Figure A.1	TM236 Frames . . . . .	48
Figure A.2	TM236 Frames . . . . .	49
Figure A.3	TM236 Frames . . . . .	50
Figure B.1	TM241 Frames . . . . .	54
Figure C.1	TM313 Frames . . . . .	58
Figure C.2	TM313 Frames . . . . .	59



## LIST OF TABLES

Table 3.1	Results of geotechnical experiments of Treuchtlinger Marmor . . . . .	7
Table 4.1	Properties of processed discs . . . . .	13
Table 5.1	Properties of "raw" videos . . . . .	15
Table 6.1	Case results TM236 . . . . .	27
Table 6.2	Case results TM241 . . . . .	31
Table 6.3	Case results TM313 . . . . .	35
Table A.1	Observations TM236 . . . . .	51
Table A.2	Observations TM236 . . . . .	52
Table B.1	Observations TM241 . . . . .	55
Table C.1	Observations TM313 . . . . .	60
Table D.1	Subjects Timetable . . . . .	62
Table D.2	Week 0 - Week 1 . . . . .	63
Table D.3	Week 2 - Week 3 . . . . .	64
Table D.4	Week 4 - Week 5 . . . . .	65
Table D.5	Week 6 - Week 7 . . . . .	66
Table D.6	Week 8 - Week 9 . . . . .	67
Table D.7	Week 10 - Week 11 . . . . .	68



# List of Algorithms

5.1	Structure of video . . . . .	15
5.2	Frames in BMP-file . . . . .	16
5.3	Cropped frames as BMP-file . . . . .	16
5.4	Absolute difference images . . . . .	17
5.5	PIVlab frames . . . . .	22



## ACRONYMS

<b>PIV</b> Particle Image Velocimetry .....	<b>3</b>
<b>UCS</b> Uniaxial Compressive Strength .....	<b>1</b>
<b>TM</b> Treuchtlinger Marmor .....	<b>2</b>
<b>BDT</b> Brazilian Disc Test .....	<b>1</b>
<b>UDG</b> Ultra Deep Geothermal .....	<b>2</b>



# 1

## INTRODUCTION

Stylolites are common geo-patterns observed in rocks in the upper crust, from geological reservoirs in sedimentary rocks to deformation zones, in folds, faults, and shear zones [Toussaint et al., 2018]. In Figure 1.1 it can be seen that they are rough surfaces and appear as rough dark lines.

Stylolites are of importance because they can affect the petrophysical characteristics (i.e. porosity/permeability) of a rock [Alsharhan and Sadd, 2000]. These stylolites have interested geoscientists for a long time primarily for the potential impact on fluid flows [Baud et al., 2016]. Toussaint et al. [2018] state that sedimentary stylolites can act as horizontal permeability barriers. Other experimental studies revealed however that stylolites in limestones do not influence permeability when they are oriented perpendicular to fluid flow but in some cases they can act as fluid conduits when orientated parallel to flow [Baud et al., 2016]. Also it has been shown that stylolites weakens a rock mass, which is supported by many observations in quarries [López-Buendía et al., 2013].

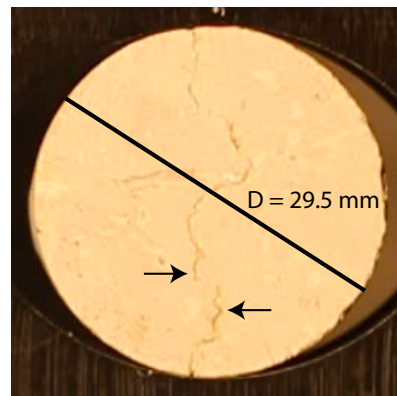


Figure 1.1: Disc of a limestone sample, cut perpendicular to the mean stylolitic plane. D indicates the diameter of the disc and the arrows indicate “teeth-like” structures.

In general, the rock physical and mechanical properties are very important parameters for geological engineering, design and construction [Peng and Zhang, 2007]. Mechanical properties include elastic properties (e.g. Young’s modulus, shear modulus, bulk modulus and Poisson’s ratio), also known as the elastic moduli, but also inelastic properties (e.g. strength and rheology). Such properties are commonly investigated using laboratory testing, where examples include the Uniaxial Compressive Strength (UCS) test, and the Brazilian Disc Test (BDT). The latter is to determine indirect tensile strength.

Geothermal energy systems have been considered as a potential alternative for fossil fuel heating. Currently, the application of geothermal energy is

not applicable for high-temperature heat (e.g. the process industry). It is anticipated that Ultra Deep Geothermal (UDG) energy could potentially make a substantial contribution to the transition towards a sustainable heat supply [Carlson, 2019]. To reach sufficiently high temperatures in the Netherlands and Germany, geothermal reservoirs at depths over 4 km are required.

In the Netherlands the Dinantian carbonate formation have great potential for Ultra Deep Geothermal (UDG). In preceding study (Pluymakers et al., pers. comm.) a series of BDT are performed on samples obtained from a quarry in the Treuchtlinger Marmor (TM), a limestone formation in southern Germany which are assumed to be equivalent to the Dinantian formation in the Netherlands (A. Pluymakers, pers. comm.). They are equivalent to each other because they are both classified as allochemical rocks and are at the same depth of approximately 4 km. The properties (see Table 3.1) from the TM limestone are found in Tamáskovics et al. [2014] and they are from a geothermal system, typical for in the western part of the Molasse Basin (see Chapter 3). The south German Molasse Basin belongs to the three regions in Germany with the highest geothermal energy potential [Tamáskovics et al., 2014].

The samples were tested using the BDT configuration. The BDT is an indirect tensile strength test which is used in rock mechanics as a test when shear needs to be minimised [López-Buendía et al., 2013]. The BDT is a widely used method for discs or ring samples. The concept is simple and is explained as follows: A circular solid disc is compressed until failure occurs [López-Buendía et al., 2013]. The direction in which uniaxially compressive stresses are applied are occurring together with the diametric fracture plane. There are four typical loading configurations as can be seen in Figure 1.2.

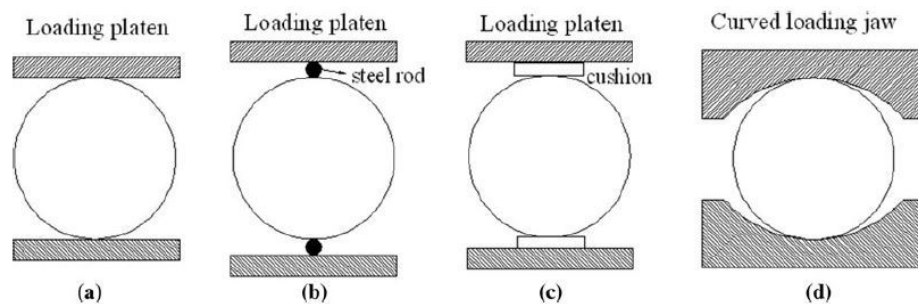


Figure 1.2: Typical Brazilian tensile test loading configurations: a) flat loading platens, b) flat loading platens with two small-diameter steel rods, c) flat loading platens with cushion, and d) curved loading jaws [Li and Wong, 2012]

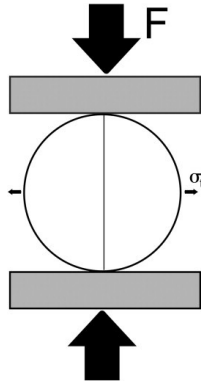


Figure 1.3: Ideal diametric fracture of a stone disc in the indirect tensile test, or Brazilian Disc Test [López-Buendía et al., 2013].

Figure 1.3 is an example of a loading plate. In the experiments described in this thesis, a curved loading jaw configuration was used.

The tensile strength is calculated with the following equation:

$$\sigma_t = \frac{F}{\pi r_0 t} \quad (1.1)$$

Where  $\sigma_t$  = Tensile strength [MPa],  $F$  = Applied force at failure [N],  $r_0$  = Radius of disc [mm] and  $t$  = Thickness of disc [mm].

The BDT permits up to cm-sized dimensions with sufficient accuracy but is very sensitive to weak points and heterogeneities [López-Buendía et al., 2013]. López-Buendía et al. [2013] states that the test is simple and effective for the evaluation of mechanical properties of a weak plane along the rock disc. In preceding study (Pluym et al., pers. comm.) videos of the BDT experiments were made with a DSLR camera. The advantage of a BDT is that we have a direct visual of the sample plane. That means that we can use photo or video images of the experiment to determine more properties of the samples in 2-D (e.g. displacement or strain field). The ratio of BDT tensile strength to hydraulic fracturing tensile strength allows prediction of the tensile strength and is an important parameter for simulation of hydraulic fracturing test results.

There are numerous methods that can be used to extract displacement and strain fields from photo or video images [Xu et al., 2011]. One method is the Particle Image Velocimetry (PIV) technique. This PIV technique has been used as a general tool to measure the displacements and, in essence, does not depend whether images correspond to fluids or solids [Xu et al., 2011]. A stylolite is a single plane of weakness. Therefore the PIV technique is a useful tool in this study to analyze the strain field of tensional failure of samples containing stylolites. PIV-based post-processing techniques were developed in recent years.

In preceding study (Pluymakers et al., pers. comm.) eleven samples with stylolites were tested, we used the data of 3 samples from this study. Note that analysing all eleven samples is outside of the scope of this study. In this study the PIV-method is used to calculate local strain rate in movies

of different limestone samples that contained a stylolite, this data is used in order to look if the stylolite orientation influences the motion of tensile failure.

The aim of this study is to develop a [PIV](#) method for highlighting strain field (2-D) in movies from the [TM](#) limestone. The second aim of this study is to look if the orientation of a stylolite influence the behaviour of strain fields and crack propagation in the [TM](#) samples.

The open source code PIVlab from [Thielicke and Stamhuis \[2014\]](#) was used in analyzing and highlighting the strain field. Details on the method used is described in [Chapter 4](#).

The knowledge obtained from the results of this report will provide helpful information about how hydraulic fracturing at micro-scale impacts rock formations (in 2-D). In particular this study can be helpful for the geothermal energy sector in Germany in the Molasse Basin or the Dinantian formation in the Netherlands. The formations are equivalent to each other because they are both classified as allochemical rocks, in what extent will be described in [Chapter 7](#).

## 2 | STYLOLITE TYPES AND CHARACTERISTICS

First we will describe characteristics and the types of a stylolite. [Toussaint et al. \[2018\]](#) summarize that stylolites appear on outcrops as rough dark lines, in numerous sedimentary rocks and in deformed zones of folds, faults, and shear zones. They are found notably, in carbonates, marbles, cherts, coals, sandstones and shales.

The dark colour (see [Figure 2.1](#)) is due to accumulation of non soluble minerals and materials (e.g. clay-rich residuals). Stylolites show mm-sized to cm-sized teeth-like structures (see (A) from [Figure 2.1](#)), pointing in the direction of largest compressive stress during their formation [[Toussaint et al., 2018](#)]. [Toussaint et al. \[2018\]](#) summarize that the size of the teeth exceeds the size of grains in the rock, which allows identification of displacement of the pre-existing structure along the sides of the teeth, showing stylolites to bound regions of undissolved material and replace the dissolved one. Stylolites present a range of sealing capacities between 63-89%, depending on their morphology, and can result in partial leakage and subsequent invasive calcitisation in their vicinity. In (B) from [Figure 2.1](#) the sealing capacity of the stylolites can be calculated defined as the ability to impede fluid flow.

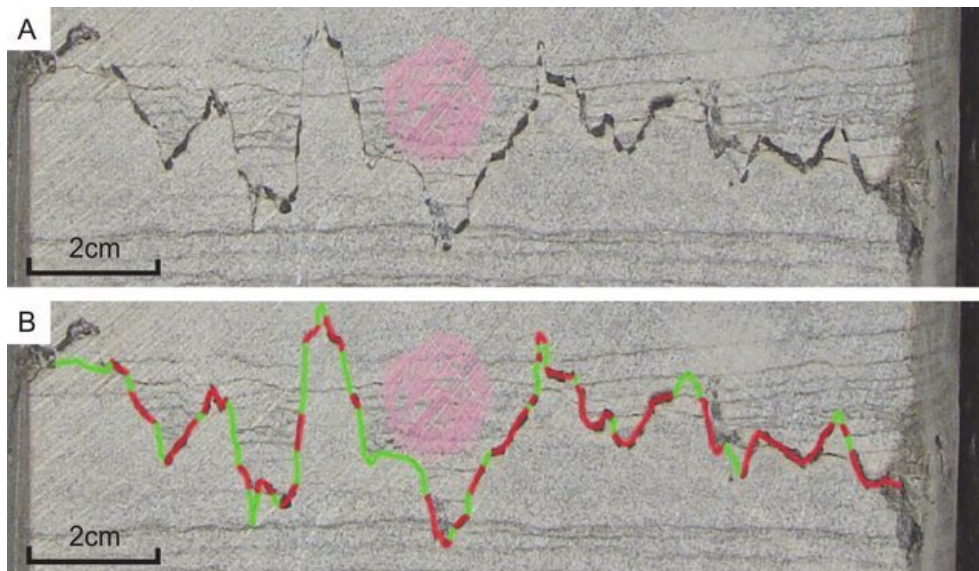


**Figure 2.1:** A. Original stylolite without interpretation B. Stylolite sealing (red) and non-sealing (green) sections measured along the total length of the stylolite to provide a sealing capacity. Stylolites are classed as sealing depending on the thickness of insoluble material. Image after [Humphrey et al. \[2019\]](#).

[Toussaint et al. \[2018\]](#) summarize that stylolites can be divided in three subcategories:

1. Sedimentary,
2. Tectonic,
3. Slickolites.

Sedimentary stylolites are oriented sub-parallel to bedding (i.e. due to overburden stress) [Baud et al., 2016]. Stylolites are secondary structures in sedimentary rocks (i.e. carbonates, cherts, coal and sandstones [Toussaint et al., 2018]). Tectonic stylolites are oriented oblique or perpendicular to bedding (i.e. due to tectonic stress) [Toussaint et al., 2018], which can be horizontal and resulting in vertical stylolites [Toussaint et al., 2018]. Slickolites develop on planes that are oblique to the largest principal stress direction [Toussaint et al., 2018]. Slickolites are inclined teeth which are not perpendicular to their average plane. Slickolites form when a stylolite grows along a pre-existing interface that is oblique to  $\sigma_1$ , the largest principal stress axis [Toussaint et al., 2018].

Bruna et al. [2019] summarize that stylolites can potentially be connected to other stylolites. In 3-D, stylolite lateral extension follows the same rules as fracture propagation [Bruna et al., 2019]. To study the stylolites in 3-D on outcrop scale, inspections can be done on only a small amount of outcrops. Therefore, not enough data has been extracted to give a clear conclusion about how stylolites are lateral extended in 3-D. Potential fluid flow in 3-D can be disconnected throughout the rock mass without knowing.

Stylolites can act as stress concentrators. [Toussaint et al., 2018]. Baud et al. [2016] found that samples with stylolites are always weaker than samples without stylolites. The stylolites most likely weakens the rock due to high porosity and permeability in and around the stylolite [Baud et al., 2016]. Baud et al. [2016] also found that if stylolites are present when tested compressional the orientation of the stylolite does not result in mechanical anisotropy. When the stylolite has a higher thickness than 5 mm, it also acts as a plane of weakness [Baud et al., 2016]. The stylolites in this study are much thinner than the 5 mm in Baud et al. [2016] and it has been found in preceding study (Pluym et al., pers. comm.) that when the stylolites are tested tensional the thickness and the mechanical anisotropy are affected by stylolites.

# 3

## PETROPHYSICAL PROPERTIES OF THE "TREUCHTLINGER MARMOR"

To understand the "Treuchtlinger Marmor", the limestone studied here, a general description of the properties of the limestone will be given here. TM is a fossil-rich limestone with a fine grained matrix. Generally speaking, limestones consists of non-skeletal grains, biogenic carbonate, matrix and cement. The components of a limestone are subdivided into skeletal material, ooids, oncolites and pellets. The age of this limestone is at about 150 million years [Hendrich, 2002]. The thickness is determined by outcrop descriptions and it is been found that the TM formation is about 50 m (see Figure 4.2). The dense matrix of the TM formation is created by microorganisms. TM has been used as a building material because the rock is easy to extract and easy to polish.

Shear strength and deformation properties				
Layer	Friction angle (°)	Cohesion c (MPa)	Young's modulus (GPa)	Poisson's ratio (0 - 1)
Treuchtlinger Marmor	38 - 41	20 - 43	28.39 - 56.86	0.13 - 0.45

Table 3.1: Shear strength and deformation properties of the TM adopted from [Tamáskovics et al., 2014].

The properties in Table 3.1 are obtained from the intact core material without stylolites of the "Treuchtlinger Marmor" [Tamáskovics et al., 2014]. This material and these properties are considered to be typical for a geothermal system in the western part of the Molasse Basin. All of the eleven samples of preceding study (Pluym et al., pers. comm.) are from the same formation and quarry, but then include stylolites. Of the different materials tested in Tamáskovics et al. [2014] as analogues for the reservoirs in the Molasse Basin the "Treuchtlinger Marmor" has shown the highest UCS, shear strength, tensile strength and Young modulus values.



# 4

## MATERIAL STUDIED AND EXPERIMENTAL SET-UP

In this chapter the origin of the material used in this study are given. Furthermore, we describe the preparation of the samples, the experimental set-up from the preceding study (Pluymakers et al., pers. comm.) (Section 4.2.1) and from this study (Section 4.2.2).

### 4.1 MATERIAL ORIGIN AND PREPARATION OF THE SAMPLES

In this study, we used TM limestones (see Figure 4.1) from Germany, which are assumed to be equivalent to the ones in the geothermal reservoirs in the Southern part of Germany [Tamáskovics et al., 2014], around Munich, as is explained in Chapter 1. They are also assumed to be equivalent to the Dinantian carbonates in the Netherlands (A. Pluymakers, pers. comm.) because the Dinantian [Carlson, 2019] and the TM carbonates [Tamáskovics et al., 2014] are both at approximately 4000 m depth. Furthermore, the in-situ temperatures of both formations are between 110 and 160 °C. Both the limestone formations can be classified as allochemical rocks. Here the Folk classification will be used. Allochemical rocks are those that contain grains brought in from elsewhere.

The "Treuchtlinger Marmor" is a transition zone between the high porosity/permeability "Neuburger Bankkalke" of the Upper Malm and the low porosity/permeability "Treuchtlinger Marmor" of the Lower Malm [Tamáskovics et al., 2014] (see Figure 4.2).



Figure 4.1: Plane section of a TM sample with a horizontal stylolite after A. Pluymakers, pers. comm.

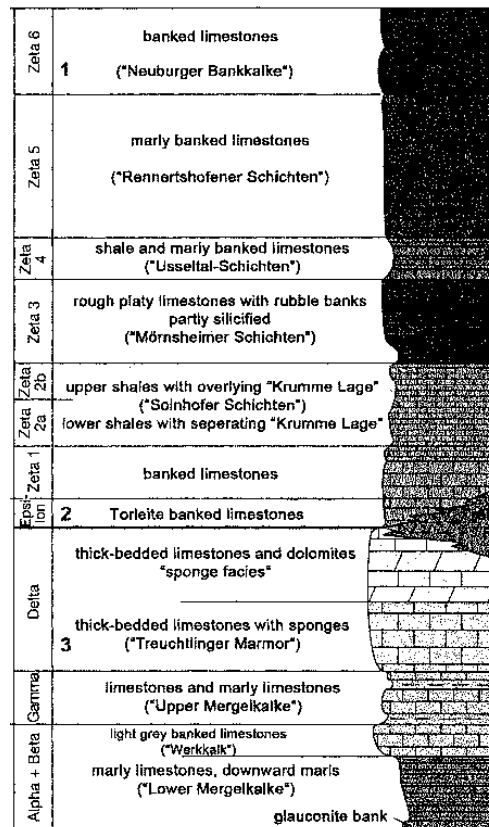


Figure 4.2: Stratigraphy of the Swabian Mountains of the Upper Jurassic from Malm alpha to Malm Zeta 6 with the Franconian Mountains lithostratigraphic units of the outcrop analogues form the Neuburger Bankkalke (1), Kelheimer Riffkalke (2), and the Treuchtlinger Marmor (3) (after state office for geology and mining Theinland-Pfalz) [Klapperich, 2014].

## 4.2 EXPERIMENTAL PROCEDURE

### 4.2.1 Procedure and results of preceding study

Eleven disc samples including stylolites with a common diameter of 29.5 mm and a thickness varying between 15 and 16 mm were prepared from the cores. And all the samples of the TM remained intact during coring.

All eleven discs were sampled which contain stylolites with four different orientations: a vertical orientation stylolite Type I and several samples at an oblique orientation to the core axis: Type II, Type III and IV. We grouped the stylolites that showed common orientation (see Figure 4.3). The angle depends on how the horizontal is defined. We choose to set the horizontal from left to right (i.e. horizontal axis). This led to the "corrected" angles which can be found in Table 4.1.

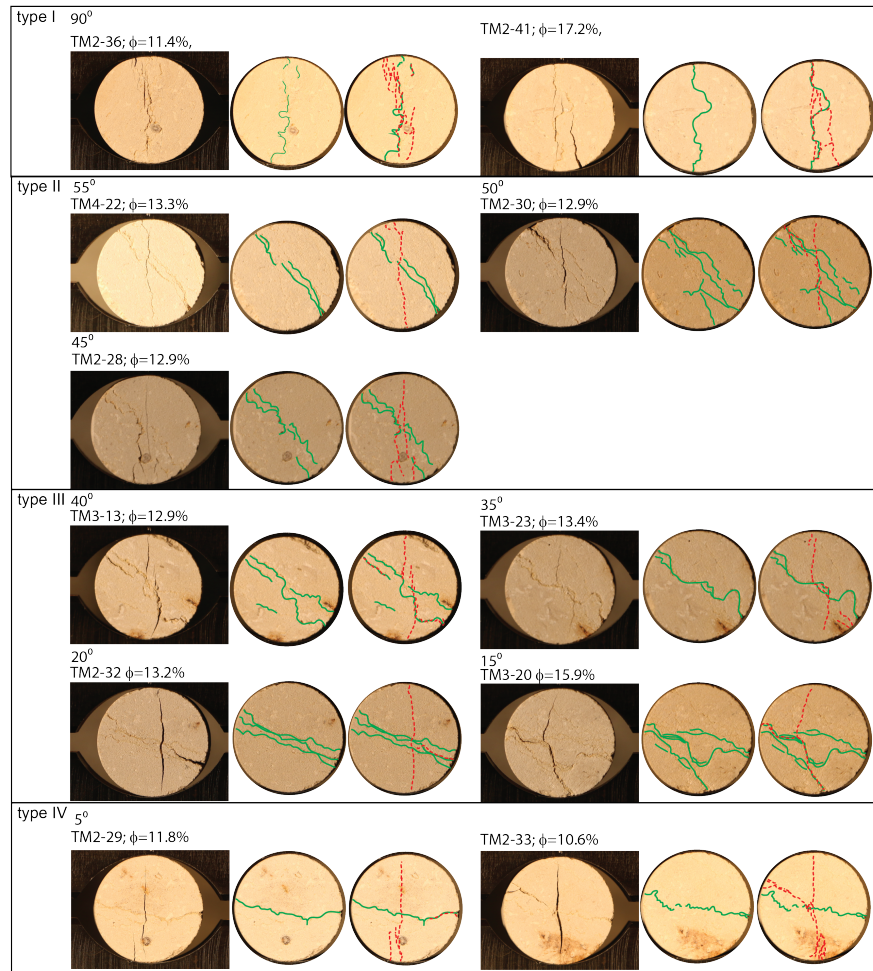


**Figure 4.3:** All eleven discs, with vertical stylolites: Type I, and oblique stylolites: Type II, III and IV. With the broken sample after the experiment on the left, in the middle the original sample with the stylolite trace in green, and on the right the broken sample with the stylolite trace in green, and in red the trace of all fractions.  $\phi$  is the porosity in percentage. Figure after A. Pluymakers, pers. comm.

#### 4.2.2 Procedure of this study

In this study we analyzed sample TM236, TM241 and TM313. Note that we only processed three of the eleven experimentally deformed discs and not all eleven. We choose those three discs because in the other 8 samples there were only one or two moments in the stress-displacement curve where there was any movement, this can be seen in Figure 4.4. Those three samples could help develop the method, and compared with each other to answer the research question. See Table 4.1 for the exact properties of the three processed discs.

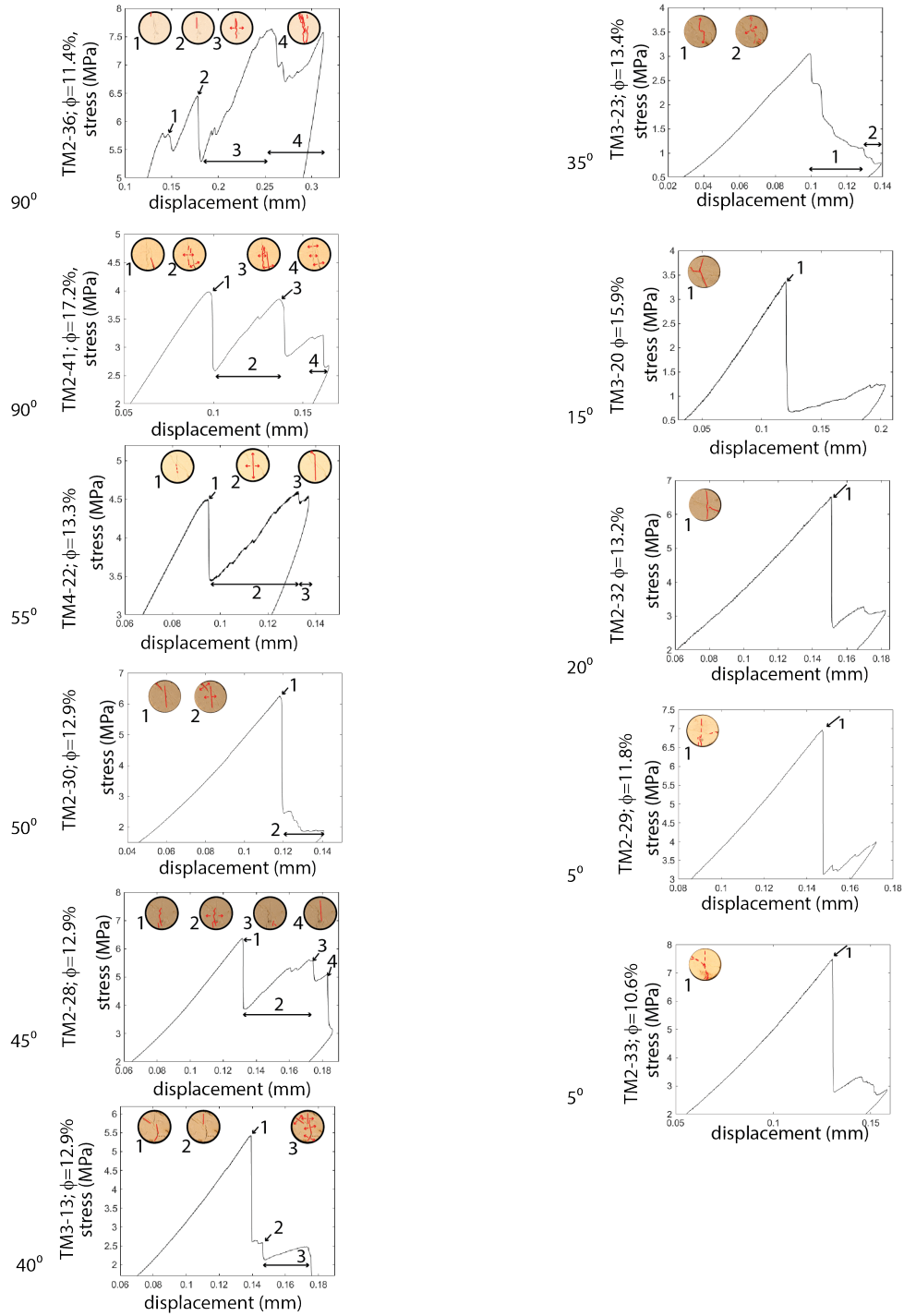


Figure 4.4: All eleven discs, with stress displacement curve. Figure after A. Pluy-makers, pers. comm.

In this study videos were made with a DSLR camera with a *Framerate* of 50 (*frames/s*). The videos from the camera were used in MATLAB to obtain all the frames in the video. More of the properties of the studied videos can be seen in Table 5.1. In Xu et al. [2011] the deformation in the experiments was recorded by the sequential digital images, this is also what we have done. We tested the following three scenarios: a) every 50 frames b) every 10

Properties of the investigated discs						
	Corrected angle (°)	Weight (g)	Diameter (mm)	Thickness (mm)	$\phi$ (%)	Type
TM236	90	25.5	29.5	15.17	11.4	I
TM241	90	24.96	29.5	15.92	17.2	I
TM313	40	25.68	29.5	15.47	12.9	III

**Table 4.1:** Properties of **TM** discs. Where I is 90° (i.e. vertical) and where III is 40° (i.e. oblique) stylolite.

frames and c) specific frames on peaks and troughs of stress-displacement curve. At first scenario a) every 10 frames and b) every 50 frames were attempted to process with PIVlab. For scenario c) a row vector in MATLAB was made which contained the frame numbers. Frame numbers were chosen such that enough displacement in PIVlab was detected. We then extracted those specific frames from the movie as a BMP-file and the frames were visually investigated (i.e. looking at the crack propagation). After this, the MATLAB PIV tool from [Thielicke and Stamhuis \[2014\]](#) was used to evaluate the motion of tensile failure in stylolite samples as described in Chapter 5. In Chapter 6 the results of the three discs from this study are analyzed and discussed.



# 5

## MOVIE PROCESSING AND PIV MODELLING

### 5.1 MOVIE PROCESSING

After loading the movies into MATLAB, frame images were made and investigated individually. The videos all have a frame width of 1280 pixels and frame height of 720 pixels.

The properties of the "raw" movies can be seen in Table 5.1. The properties were extracted with a MATLAB code.

Properties of the videos				
	Duration (s)	Frame Rate (frames/s)	Total Frames (frames)	
TM236	278.4	50	13920	
TM241	140.32	50	7016	
TM313	126.84	50	6300	

Table 5.1: Properties of "raw" videos

Initially the movies were a MOV-file, however due to contrictions in the MATLAB version used, the movies were converted to an AVI-file. After extracting all the properties, the movies were individually put into a MATLAB structure (see Algorithm 5.1). From here the total frames (see Table 5.1) were extracted for every video.

---

**Algorithm 5.1:** Structure of a Video Object

---

**Input:** A Video Object

**Output:** Frames into a structure

```
1 while hasFrame(vidObj) do
2   for k = 1 do
3     mov(k).cdata = readFrame(vidObj);
4     k+1;
5   end
6 end
```

---

After creating a structure with the frames in there we could extract every possible frame and save them as a BMP-file (see Algorithm 5.2). This is done because the BMP-file format is capable of storing 2-D digital images both monochrome and color, in various color depths [Wikipedia, 2020]. This is important because stylolites mainly occur in 2-D, in this study as well where we calculate the local strain rate which is also in 2-D.

---

**Algorithm 5.2:** Frames saved as BMP-file in specific folder

---

**Input:** Total Frames**Output:** BMP-file of the specific frame

```

1 for x = 1:k do
2   thisFrame = mov(x).cdata;
3   outputBaseFileName = sprintf('Frame %4.4d.bmp', x);
4   outputFullFileName = fullfile(outputFolder,
   outputBaseFileName);
5   imwrite(thisFrame, outputFullFileName, 'bmp');
6   end

```

---

Note that for specific ranges of frame(s), the for-loop could be changed.

Because we only need the strain rate in the samples and not in the machinery, we cropped the image. This allows us to measure only the strain rate in a smaller image. In order to crop the image we used the following MATLAB code (see Algorithm 5.3):

---

**Algorithm 5.3:** Cropped frames saved as BMP-file in specific folder

---

```

1 D = 'directory where the files are saved';
2 images = dir(fullfile(D, '*.bmp'));
3 N = length(images);
4 I = imread(images(1).name);
5 (x, rect) = imcrop(I);
6 outputcropped = 'directory where the files will be saved';
   Input: Images of frames
   Output: Cropped images of frames
7 for i = 1:N do
8   I = imread(images(i).name);
9   I = imcrop(I, rect);
10  fullFileName = fullfile(outputcropped, images(i).name);
11  imwrite(I, fullFileName);
12  end

```

---

After using Algorithm 5.3 we get Figure 5.1.

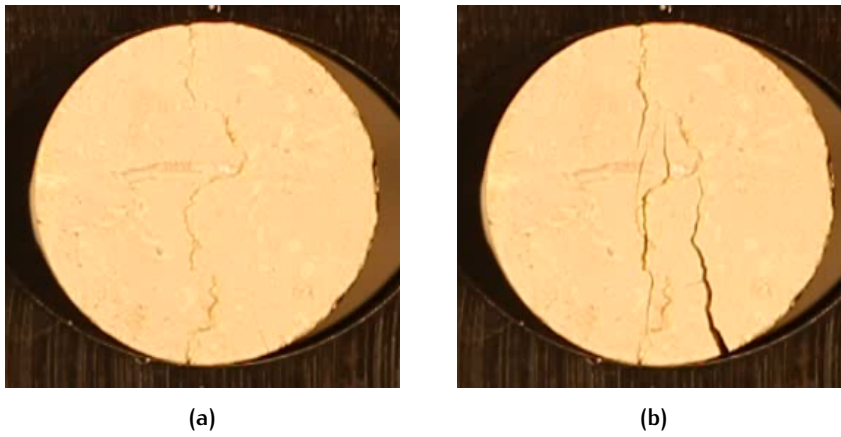


Figure 5.1: Example of an image for the cropped frames, specifically the first frame from the row vector: (a) Cropped Frame 2900 is at 58 seconds of TM241 movie. And the last frame from the row vector (b) Cropped Frame 6190 is at 123.8 seconds of TM241 movie.

To validate if the movement was correlated with the PIVlab frames in Section 5.2, images were subtracted. This provides a clear visual to determine where the movement took place (see Figure 5.2). To make it clearly visible the following MATLAB code was used (see Algorithm 5.4):

---

**Algorithm 5.4:** Absolute difference of images  $n$  to  $n+1$

---

**Input:** Images

**Output:** Subtracted images

```

1 for  $n = 1:N$  do
2   img = imread(croppedimages(n).name);
3   compareimg = imread(croppedimages(n+1).name);
4   P = imabsdiff(img,compareimg);
5   BW1 = im2bw(P, 0.02);
6   BW1im = imcomplement(BW1);
7   fig = figure(n);
8   hold off
9   imshow(BW1im, []);
10  hold on
11  axis equal tight off
12  end

```

---

The native Matlab command 'im2bw' replaces all pixels in the input image with luminance greater than level with the value 1 (white) and replaces all other pixels with the value 0 (black). An level value of 0.02 is used because after trial and error this value gives the clearest result. The black pixels are indicating displacement in the frame and the white pixels are indicating that pixels stay on the same place with respect to their 'before' image.

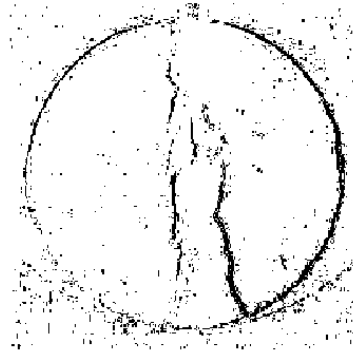


Figure 5.2: Example of an image for the absolute difference, specifically frame 5136 and 5801 from TM241 movie

## 5.2 PARTICLE IMAGE VELOCIMETRY MODELLING

To determine the displacement distributions on the surface of the **TM** discs, digital videos of the discs were taken and evaluated with an image analysis technique, called **PIV**. The raw video images were first converted into ones in a readable format. The frame images were then extracted from the readable video images [Xu et al., 2011] (see Section 5.1).

In this study a software tool of the **PIV** theory using MATLAB scripts, called PIVlab was used. It calculates the velocity distribution within frame-pairs, but can also be used to derive, display and export multiple parameters [Thielicke and Stamhuis, 2014] of the flow pattern, such as calculating the strain rate on the limestone images with stylolites. The tensile displacements were defined as positive numbers [Xu et al., 2011] and compression is defined as negative numbers.

### 5.2.1 Background theory of the PIVlab tool

In PIVlab, the displacement in a sample is measured in the plane of the image and inferred from two consecutive images (i.e. frame), separated by a time distance [Xu et al., 2011].

Equation 5.1 is used for determining the strain within a rock:

$$\epsilon = \frac{\Delta L}{L_0} \quad (5.1)$$

Where  $\epsilon$  = Strain [-],  $L_0$  = Original length of the rock [mm] and  $\Delta L$  = Change in length [mm]

Strain is positive if the rock particles are stretched and negative if they are compressed.

In the PIVlab toolbox the strain rate was determined by using the actual diameter of the samples of 29.5 *mm* and the time step between the images. The strain rate can be calculated by equation 5.2:

$$\dot{\epsilon} = \frac{d\epsilon}{dt} = \frac{d}{dt} \left( \frac{\Delta L}{L_0} \right) = \frac{1}{L_0} \frac{\Delta L}{dt}(t) = \frac{v(t)}{L_0} \quad (5.2)$$

Where  $v(t)$  is the speed at which the ends of the rock are moving away from each other [mm/s] and  $\dot{\epsilon}$  is the strain rate [ $s^{-1}$ ].

### 5.2.2 Procedure PIVlab

First, some images were loaded and sequencing style was set to 1-2, 2-3, 3-4. The images were loaded in this order into PIVlab. Each sub-window in the first image was compared with a sub-window in the second image [Xu et al., 2011]. Because all the digital images have a different time distance between each other, only 2 images could be processed at a time.

Only a small part of the image needed to be analysed and not the whole image, thus a region of interest (ROI) was selected by hand. Additionally, a mask was manually drawn and applied to exclude the area in the image which should not be analysed (i.e. the area surrounding the disc). This mask was saved and applied on all images from the same movie.

In PIVlab the correlation algorithm 'FFT window deformation' was used. Using this algorithm, the data was analysed in several passes: The first pass uses relatively large interrogation areas to calculate the displacement of the image data reliably. In Thielicke and Stamhuis [2014], they state that larger interrogation areas result in better signal-to-noise ratio and consequently result in more robust cross correlations. However, larger interrogation areas will give a very low velocity vector resolution (i.e. velocity vectors per frame). Therefore, the size of the interrogation windows was decreased gradually. The displacement information of the first pass is used to offset the interrogation areas in the second pass and so on [Thielicke and Stamhuis, 2014]. This gradually decrease of interrogation areas results in high velocity vector resolution, a high signal-to-noise ratio, and a high dynamic velocity range. In this study three passes were used starting with big interrogation areas of 64 pixels to 32 pixels and ending with a small interrogation area of 16 pixels. PIVlab utilized 50 percent overlap of the sub-windows. The more passes you use, the better will be the result. However, if the number of passes becomes too high, with a standard laptop, it will take too long to compute the displacement information. Therefore, we opted for three passes in this study.

Secondly, the frames were calibrated for distance, where the reference distance was selected by selecting the upper and the lower edge of the disc. Then the real diameter (i.e. from upper to lower edge of the disc) of 29.5 (*mm*) was entered, with which PIVlab can determine how many pixels there are in one meter.

As input for the sequencing set, we tested three scenarios:

- (a) Every 10 frames

(b) Every 50 frames

(c) Specific frames on peaks and troughs of stress-displacement curve

Frame numbers for scenario c) are indicated in the stress-displacement curves (see Figure 5.3 and Figure 5.4).

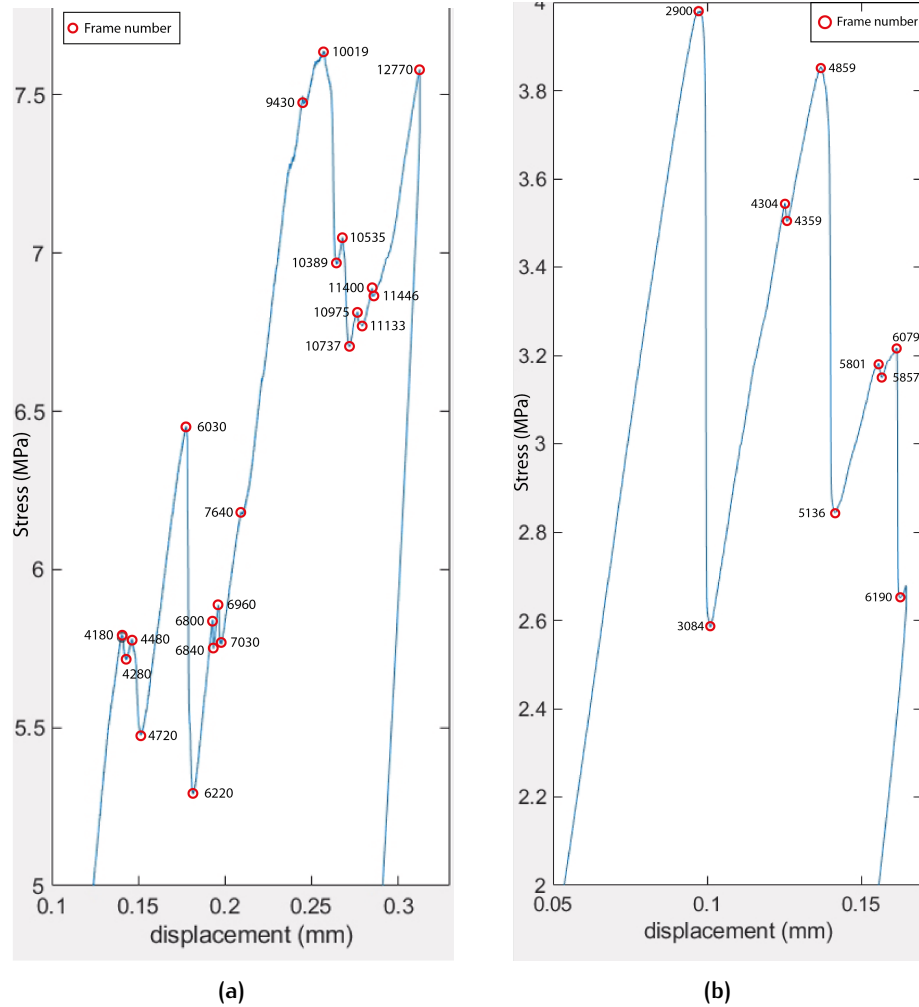
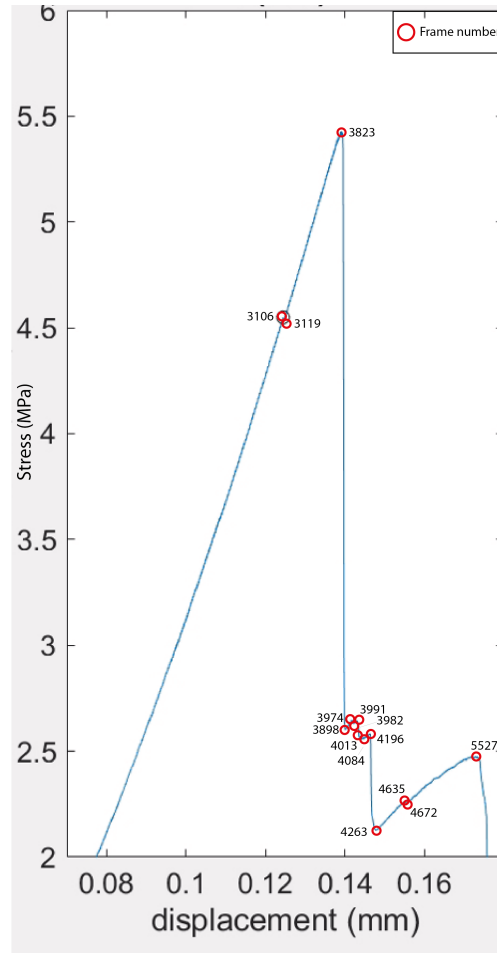


Figure 5.3: (a) Stress displacement curve TM236 (b) Stress displacement curve TM241. The numbers are the frame numbers in the movie in the peaks and the troughs. We used a red circle to highlight the peaks and the troughs.



**Figure 5.4:** (c) Stress displacement curve TM313. The numbers are the frame numbers in the movie in the peaks and the troughs. We used a red circle to highlight the peaks and the troughs.

Using the three scenarios the time step between the framepairs was determined in MATLAB using Equation 5.3 and put into PIVlab.

$$\text{Framerate} = \text{FPS}(\text{FramesPerSecond}) = \frac{\Delta \text{frames}}{\Delta t} \quad (5.3)$$

Where *Framerate* = rate with which the movie is recorded [frames/s],  $\Delta \text{frames}$  = Amount of frames [Frames] between a time step  $\Delta t = [\text{s}]$

The PIVlab toolbox delivers images with color codes indicating extension (yellow) and compression (blue) of rock particles overlain by the velocity vectors indicated with arrows (black). Note that black velocity vectors are bigger where the displacement is larger. Furthermore, the data was validated by setting velocity limits. We saw that some erroneous velocity vectors showed up due to poorly illuminated regions in the image or strong out-of-plane flow (i.e. generating excessive errors) [Thielicke and Stamhuis, 2014]. Therefore the outliers were discarded in the scatter-plot. In the frame interpolated velocity vectors are displayed in orange (see Figure 5.5).

Finally, the strain rate was extracted from each frame and saved for further processing in MATLAB.

In Figure 5.5 a typical result for scenario c) of the PIVlab toolbox can be seen. After this the strain rate values were exported to MATLAB and used in Algorithm 5.5.

In Algorithm 5.5 the code is given for processing the frames from PIVlab with using Equation 5.1 and Equation 5.2 in MATLAB:

---

**Algorithm 5.5:** Processing PIVlab frames

---

**Input:** Frames of PIVlab

**Output:** Frames of PIVlab with c-axis

```

1 for i = 1:N do
2   h=figure; imshow(images(i).name);
3   c = colorbar
4   c.Label.String = 'Strain rate (s-1);
5   caxis([minstrain maxstrain])
6   hold on
7   axis equal tight off
8   end

```

---

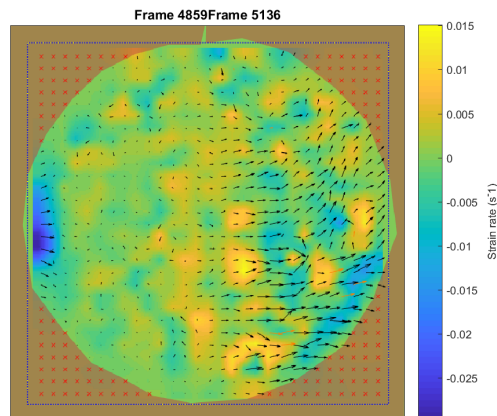


**Figure 5.5:** Example of an image for the PIVlab result for scenario c) row vector for specific frames, after using Algorithm 5.5 specifically Frame 4859-5136 from TM236 movie. The blue colour indicates negative strain rate and yellow colour is positive strain rate. Black velocity vectors can be seen in the figure and are bigger where the displacement is larger. Interpolated velocity vectors are indicated in orange.

In the last processing step, the results from the image subtraction and the PIVlab tool for each framepair are plotted in one figure and compared. This is reported in Chapter 6. Note that we used the software "Adobe Illustrator" to highlight the disc and the stylolite in a red colour.

# 6

## RESULTS AND ANALYSIS FROM DATA-SET

In this section the results of the model are given and compared with each other. We analyzed TM236, TM241 and TM313 movies and the results are described in Section 6.2.1, Section 6.2.2 and Section 6.2.3, respectively. For all the figures and tables we refer to Appendix A, Appendix B and Appendix C.

### 6.1 RESULTS OF SCENARIO A) 10 FRAMES AND B) 50 FRAMES

Choosing framepairs such that frame 1 and 2 were 10 of the original movieframes apart (0.2 sec) or 50 of the original movieframes apart (1 sec), results in random noise. There is no distinction possible between motion location (see Figure 6.1 and Figure 6.2). However, the velocity vectors are already more clearly defined for every 50 frames than for every 10 frames.

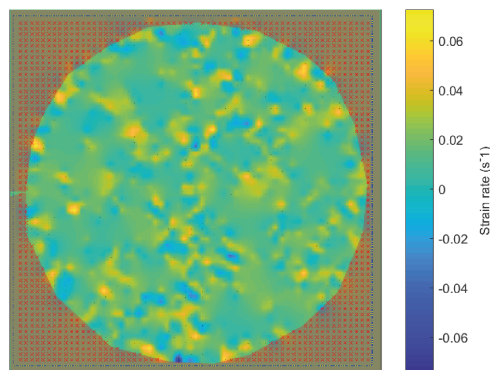


**Figure 6.1:** Example of a PIVlab result for scenario a) every 10 frames, specifically Frame 3000-3010 from TM236 movie. The blue part is negative strain rate and the yellow part is positive strain rate. Velocity vectors can be seen in the figure and are bigger where the displacement is larger.

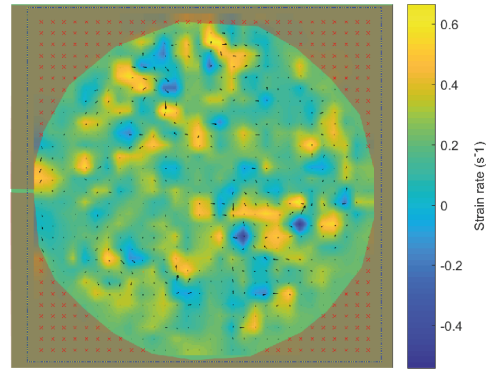


**Figure 6.2:** Example of a PIVlab result for scenario b) every 50 frames, specifically Frame 2910-2960 from TM241 movie. The blue part is negative strain rate and the yellow part is positive strain rate. Velocity vectors can be seen in the figure and are bigger where the displacement is larger.

Therefore, the results of scenario a) and b) were discarded and only scenario c) was used.

## 6.2 RESULTS OF SCENARIO C) SPECIFIC FRAMES

When we tested the images from the first peak and the first trough PIVlab noticed enough displacement to give an accurate result. In Section 6.2.1, Section 6.2.2 and Section 6.2.3 the results of this scenario on the three tested samples are described. Two consecutive frames (i.e. 'before' and 'after') per case are analysed. In all the result sections the framepairs for the common cases are chosen which are most obvious.

There are three common cases (which are deducted from Table A.1, Table A.2, Table B.1 and Table C.1 in the Appendices).

1. Random extension and compression: positive and negative strain rate are randomly distributed in the sample. See example in Figure 6.3.
2. Asymmetric extension: positive strain rate occurs in between stylolite and crack. See example in Figure 6.4.
3. Symmetric extension: positive strain rate occurs around stylolite. See example in Figure 6.5.

After identifying the three common cases (Case 1, Case 2 and Case 3), we will correlate their occurrence with their location on the stress-displacement curves. Moreover, we have also identified which framepairs yielded on average the highest strain rates, which we have indicated with an orange overlay on the corresponding part of the stress-displacement curves. In the following sections, we will describe the results of choosing the different framepairs.

### 6.2.1 Results for a 90 degree stylolite (TM236)

As there can be seen in (D) from Figure 6.4 the strain rate is the highest between where the crack initiate and the stylolite on the left side, between the crack and the stylolite the material particles stretches the most and has therefore a positive strain rate. Furthermore, the crack propagates throughout the stylolite region and has therefore a vertically oriented crack. Below the common cases are analyzed (see Table 6.1) and described in a qualitative way. The highest negative and positive strain rate are  $-0.008 \text{ s}^{-1}$  and  $0.004 \text{ s}^{-1}$ .

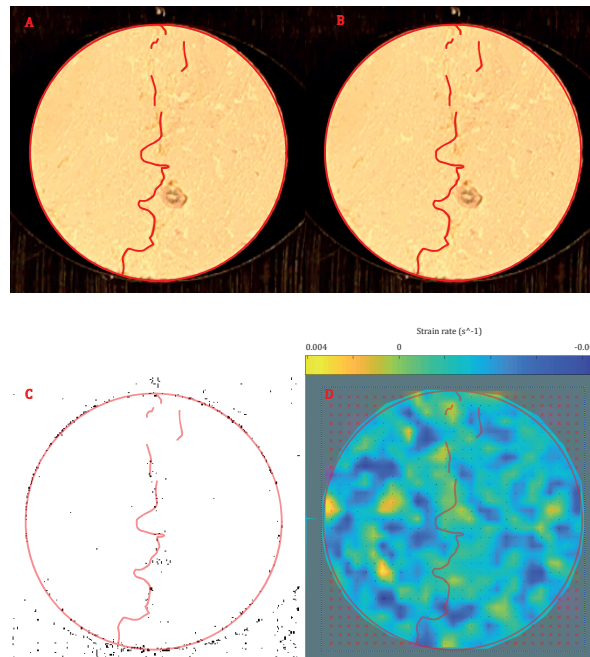


**Figure 6.3: Case 1:** (A) 'Before' Image 4180 is at 83.6 seconds and (B) 'After' Image 4280 is at 85.6 seconds. In (C) is the absolute difference between image 4180 and image 4280. This is where the particle movement (e.g. crack) of the 'After' image relative to the 'Before' image is indicated in black. In (D) is the processed frame in PIVlab and above D, the strain rate is in ( $\text{s}^{-1}$ ). In red the initial place of the stylolite is indicated, as well as the circumference.

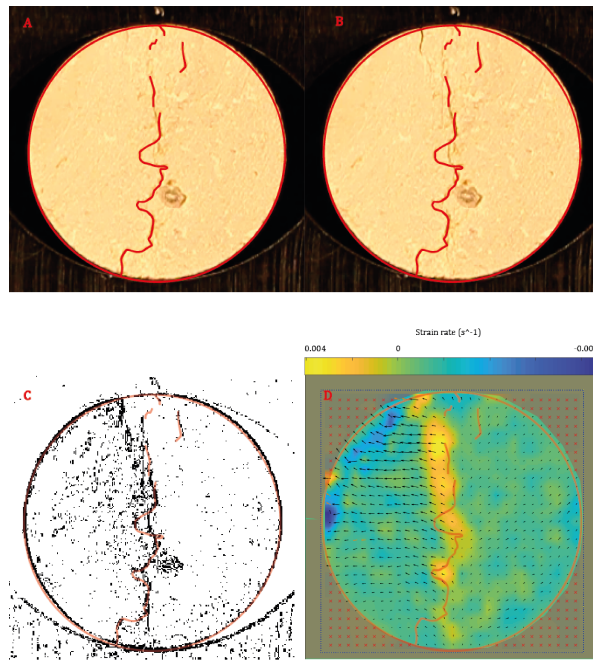


**Figure 6.4: Case 2:** (A) 'Before' Image 4720 is at 94.4 seconds and (B) 'After' Image 6030 is at 120.6 seconds. In (C) is the absolute difference between image 4720 and image 6030. This is where the particle movement (e.g. cracks) of the 'After' image relative to the 'Before' image is indicated in black. In (D) is the processed frame in PIVlab and above D, the strain rate is in ( $s^{-1}$ ). In red the initial place of the stylolite is indicated, as well as the circumference.

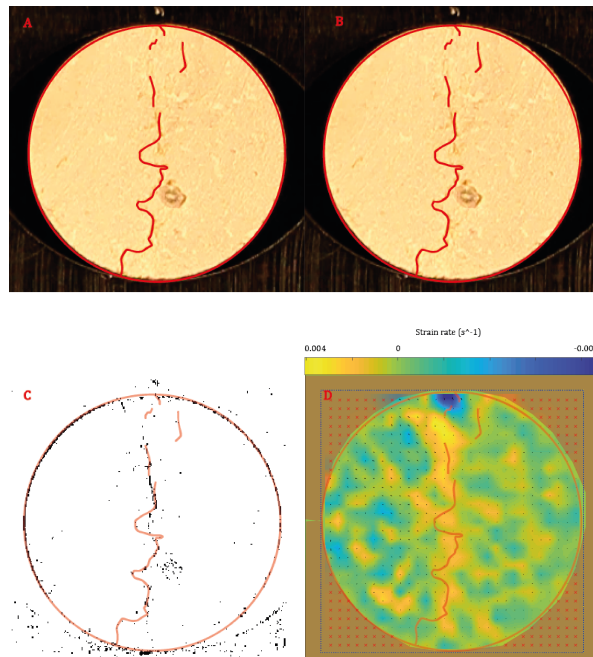


**Figure 6.5: Case 3:** (A) 'Before' Image 4280 is at 85.6 seconds and (B) 'After' Image 4480 is at 89.6 seconds. In (C) is the absolute difference between image 4280 and image 4480. This is where the particle movement (e.g. crack) of the 'After' image relative to the 'Before' image is indicated in black. In (D) is the processed frame in PIVlab and above D, the strain rate is in ( $s^{-1}$ ). In red the initial place of the stylolite is indicated, as well as the circumference.

For TM236 movie, we mainly encounter Case 1, i.e. random noise (see Table 6.1). This happens mainly with a negative  $\Delta Stress/\Delta Disp$ . We encounter Case 2 (i.e. Assymmetric extension) mainly when the  $\Delta Stress/\Delta Disp$  is positive. Case 2 have the highest positive  $\Delta Stress$  values. And Case 3 (i.e. Symmetric extension) only occurs twice. Case 3 can both have a negative or positive  $\Delta Stress/\Delta Disp$ .

cases TM236				
Region of frames	Case	$\Delta Stress/\Delta Disp$ (Positive or Negative)	$\Delta Stress$ (MPa)	
4180 - 4280	1	Negative	-0.1	
4280 - 4480	3	Positive	+0.08	
4480 - 4720	1	Negative	-0.3	
4720 - 6030	2	Positive	+0.9	
6030 - 6220	1	Negative	-1.06	
6220 - 6800	2	Positive	+0.52	
6800 - 6840	1	Negative	-0.1	
6840 - 6960	2	Positive	+0.14	
6960 - 7030	1	Negative	-0.12	
7030 - 7640	2	Positive	+0.4	
7640 - 9430	2	Positive	+1.24	
9430 - 10019	2	Positive	+0.14	
10019 - 10389	3	Negative	-0.64	
10389 - 10535	1	Positive	+0.08	
10535 - 10737	1	Negative	-0.32	
10737 - 10975	1	Positive	+0.1	
10975 - 11133	1	Negative	-0.04	
11133 - 11400	1	Positive	+0.1	
11400 - 11446	1	Negative	-0.02	
11446 - 12770	1	Positive	+0.68	

**Table 6.1:** Cases results of TM236 strain rate in frames. Where  $\Delta Stress/\Delta Disp$  is the stress drop, negative is downwards and positive is upwards. And where MPa is the amount of MPa increase (i.e. positive) or decrease (i.e. negative). Both seen in the stress displacement curve. The cases are described in the introduction of Chapter 6.

As there can be seen in Figure 6.6a the most particle displacement is mainly in the positive  $\Delta Stress/\Delta Disp$ . Furthermore, as there can be seen in Figure 6.6b Case 2 occurs exclusively on the way up, and Case 1 and 3 are more often on the way down, though also on the way up. There is no clear correlation with displacement. Case 1 is observed in the first highest negative  $\Delta Stress/\Delta Disp$  (i.e. after the linear phase of the stress-displacement curve). Case 3 is observed in the second highest negative  $\Delta Stress/\Delta Disp$ .

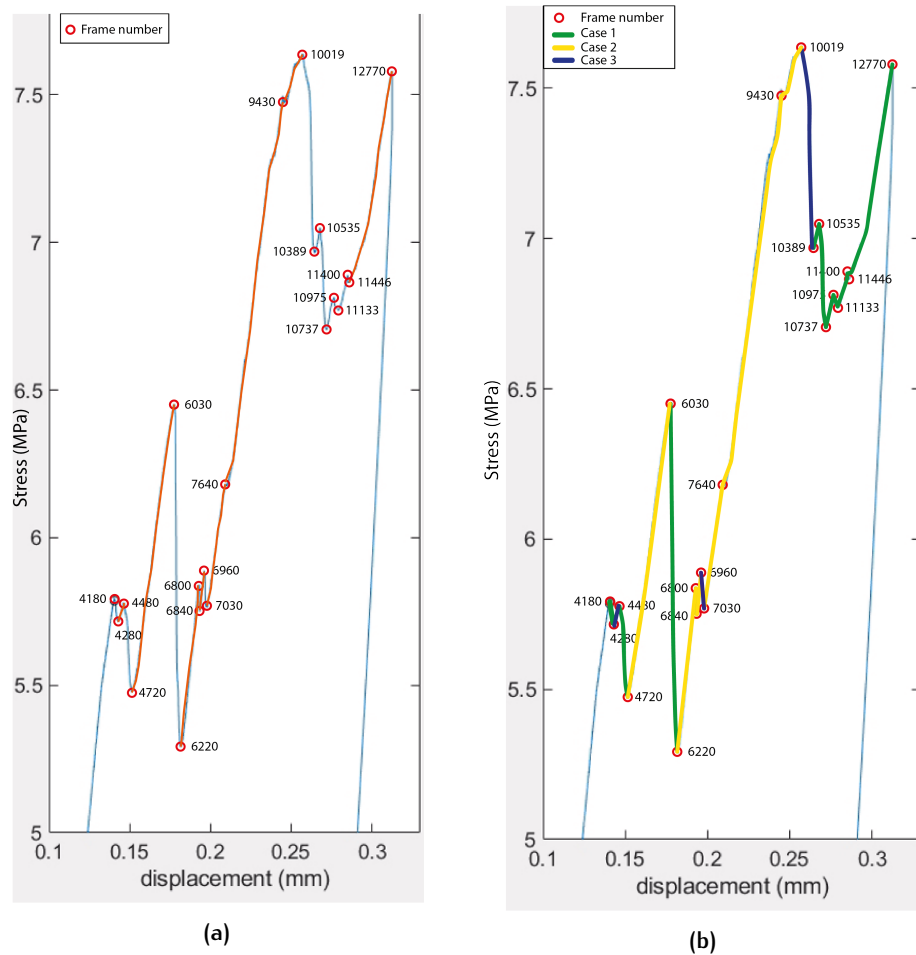


Figure 6.6: (a) The red circles are the frame numbers extracted in the peaks and the troughs and the orange lines are the parts where the most activity takes place. (b) The green lines indicate Case 1, the yellow lines indicate Case 2 and the blue lines indicate Case 3.

### 6.2.2 Results for a 90 degree stylolite (TM241)

As there can be seen in (D) from Figure 6.8 the strain rate is the highest between where the primary crack and secondary crack initiates and the stylolite. However, high strain rate can also be observed throughout the whole sample. This can also be observed in (D) from Figure 6.9.

Furthermore, the crack propagates between the stylolite bending regions and propagates as a vertically oriented crack. The primary cracks propagates vertically until the stylolite is reached. The secondary crack propagates vertically in the middle of the stylolite where there is a bending.

Also, in Figure 6.10a in orange is indicated where the most displacement takes place. The highest negative and positive strain rate is  $-0.025 \text{ s}^{-1}$  and  $0.015 \text{ s}^{-1}$  respectively.

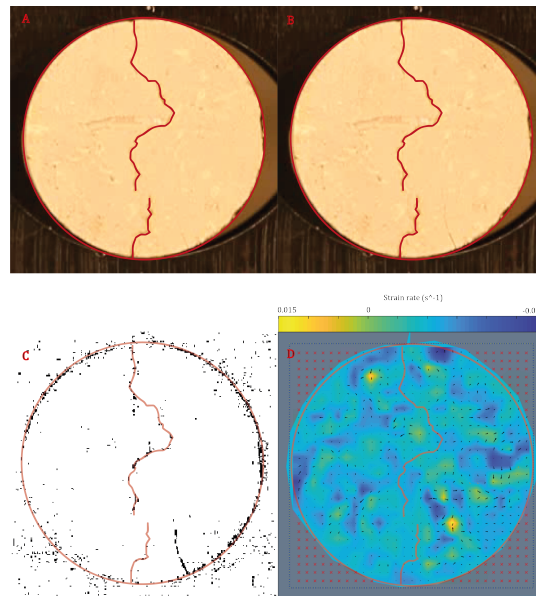


**Figure 6.7: Case 1:** (A) 'Before' Image 2900 is at 58 seconds and (B) 'After' Image 3084 is at 61.68 seconds. In (C) is the absolute difference between image 2900 and image 3084. This is where the particle movement (e.g. crack) of the 'After' image relative to the 'Before' image is indicated in black. In (D) is the processed frame in PIVlab and above D, the strain rate is in ( $s^{-1}$ ). In red the initial place of the stylolite is indicated, as well as the circumference.

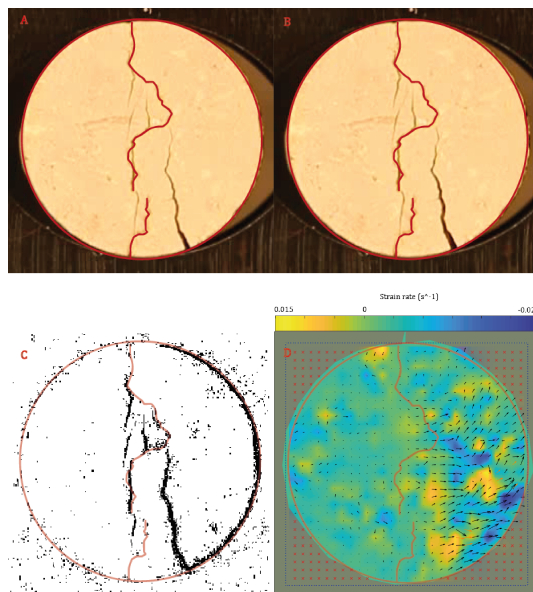


**Figure 6.8: Case 2:** (A) 'Before' Image 5857 is at 117.14 seconds and (B) 'After' Image 6079 is at 121.58 seconds. In (C) is the absolute difference between image 5857 and image 6079. This is where the particle movement (e.g. crack) of the 'After' image relative to the 'Before' image is indicated in black. In (D) is the processed frame in PIVlab and above D, the strain rate is in ( $s^{-1}$ ). In red the initial place of the stylolite is indicated, as well as the circumference.

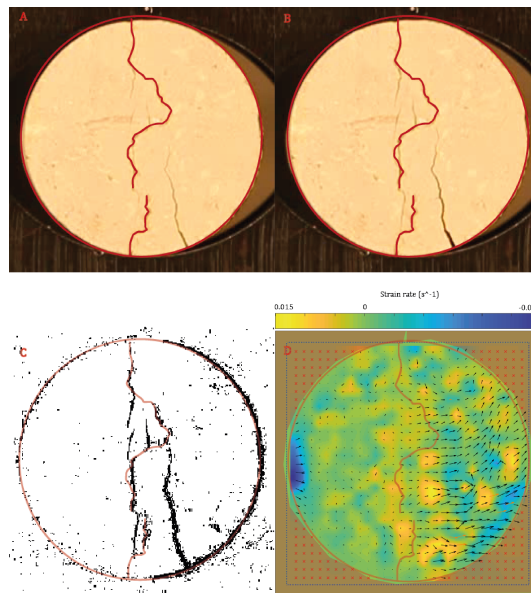


**Figure 6.9: Case 3:** (A) 'Before' Image 4859 is at 97.18 seconds and (B) 'After' Image 5136 is at 102.72 seconds. In (C) is the absolute difference between image 4859 and image 5136. This is where the particle movement (e.g. crack) of the 'After' image relative to the 'Before' image is indicated in black. In (D) is the processed frame in PIVlab and above D, the strain rate is in ( $s^{-1}$ ). In red the initial place of the stylolite is indicated, as well as the circumference.

For TM241 movie, we mainly encounter Case 1, i.e. random noise (see Table ??). This happens mainly with a negative  $\Delta Stress/\Delta Disp$ . We encounter Case 2 (i.e. Assymmetric extension) mainly when the  $\Delta Stress/\Delta Disp$  is positive, and Case 3 (i.e. Symmetric extension) only occurs twice. Case 3 can both have a negative or positive  $\Delta Stress/\Delta Disp$ . Also, Case 1 and 3 have the highest  $\Delta Stress$  values.

cases TM241				
Region of frames	Case	$\Delta Stress / \Delta Disp$ (Positive or Negative)	$\Delta Stress$ (MPa)	
2900 - 3084	1	Negative	-2.3	
3084 - 4304	3	Positive	+1.6	
4304 - 4359	1	Negative	-0.075	
4359 - 4859	1	Positive	+0.58	
4859 - 5136	3	Negative	-1.65	
5136 - 5801	2	Positive	+0.58	
5801 - 5857	1	Negative	-0.05	
5857 - 6079	2	Positive	+0.1	
6079 - 6190	1	Negative	-0.93	

**Table 6.2:** cases results of TM241 strain rate in frames. Where  $\Delta Stress / \Delta Disp$  is the stress drop, negative is downwards and positive is upwards. And where MPa is the amount of MPa increase (i.e. positive) or decrease (i.e. negative) in the stress displacement curve. The cases are described in the introduction of 6.

As there can be seen in Figure 6.10a the most particle displacement is mainly in the positive  $\Delta Stress / \Delta Disp$ . Furthermore, as there can be seen in Figure 6.10b Case 2 occurs exclusively on the way up, and Case 1 and 3 are more often on the way down, though also on the way up. There is no clear correlation with displacement. Case 1 is observed in the first highest negative  $\Delta Stress / \Delta Disp$  (i.e. after the linear phase of the stress-displacement curve). Case 3 is observed in the second highest negative  $\Delta Stress / \Delta Disp$ .

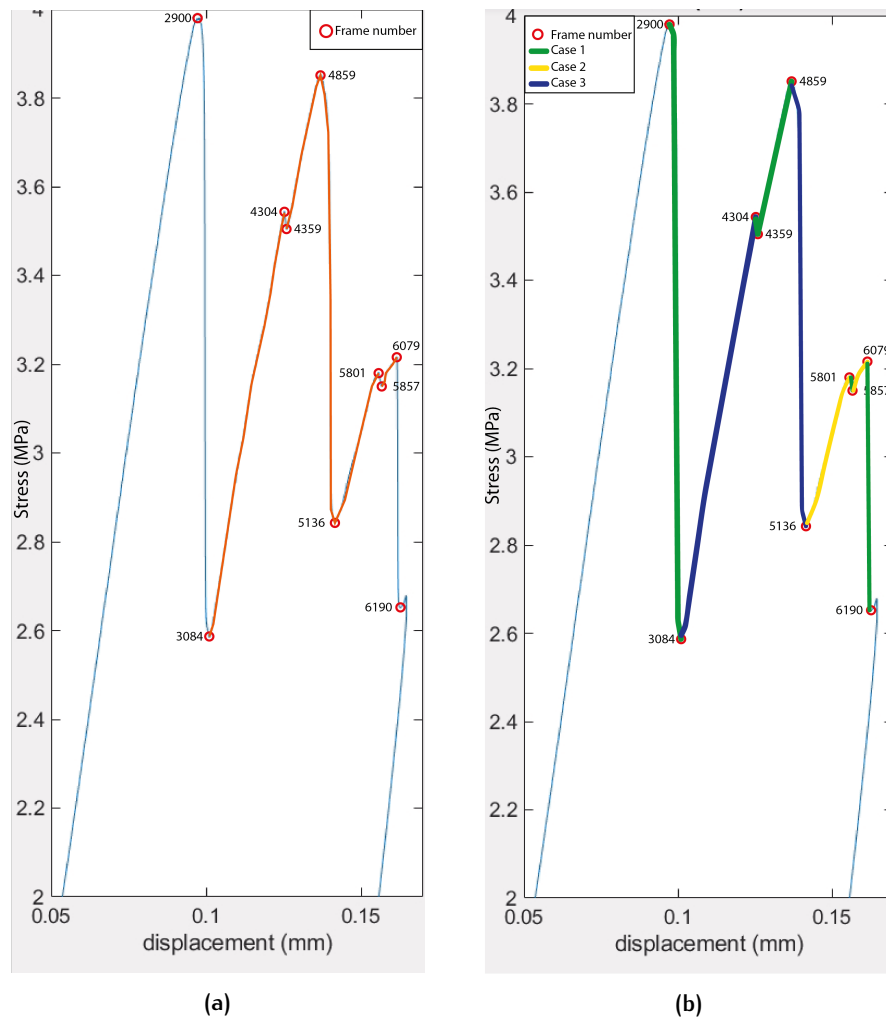


**Figure 6.10:** (a) The red circles are the frame numbers extracted in the peaks and the troughs and the orange lines are the parts where the most activity takes place. (b) The green lines indicate Case 1, the yellow lines indicate Case 2 and the blue lines indicate Case 3.

### 6.2.3 Results for a 40 degree stylolite (TM313)

High strain rate can also be observed throughout the whole sample. This can also be observed in (D) from Figure 6.11. However, as there can be seen in (D) from Figure 6.12 the strain rate is the highest where the 2 main cracks initiate and the stylolite.

Furthermore, the cracks are seen to curve towards the stylolite. Also the crack propagate as a vertically oriented crack. It is seen that the primary and secondary cracks propagates vertically in the center of the sample.

In Figure 6.14a in orange is indicated where most displacement takes place. The highest negative and positive strain rates are  $-0.03 \text{ s}^{-1}$  and  $0.01 \text{ s}^{-1}$  respectively.

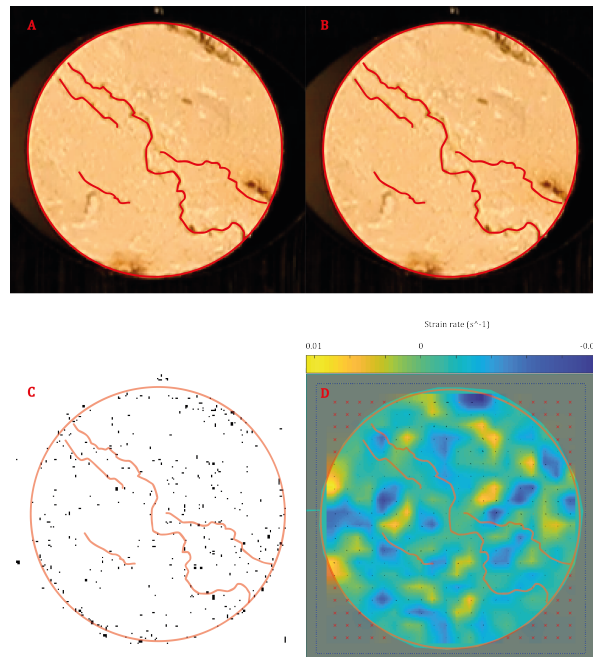


**Figure 6.11: Case 1:** (A) 'Before' Image 3106 is at 62.12 seconds and (B) 'After' Image 3119 is at 62.38 seconds. In (C) is the absolute difference between image 4720 and image 6030. This is where the particle movement (e.g. crack) of the 'After' image relative to the 'Before' image is indicated in black. In (D) is the processed frame in PIVlab and above D, the strain rate is in ( $s^{-1}$ ). In red the initial place of the stylolite is indicated, as well as the circumference.

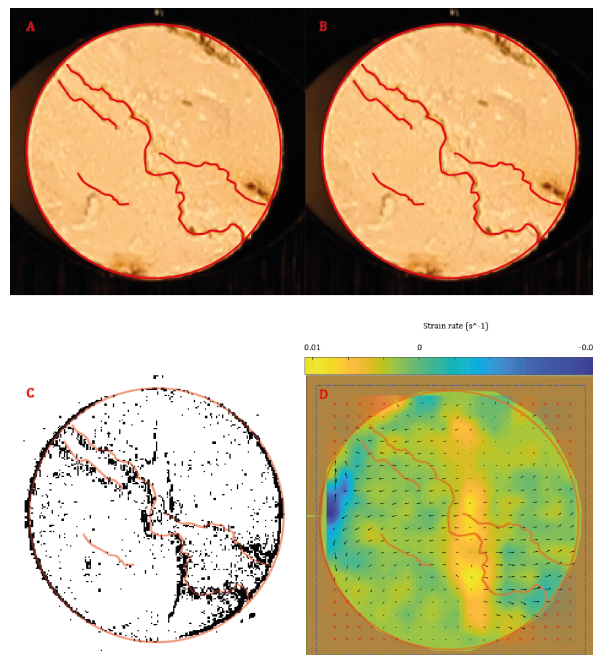


**Figure 6.12: Case 2:** (A) 'Before' Image 3823 is at 76.46 seconds and (B) 'After' Image 3898 is at 77.96 seconds. In (C) is the absolute difference between image 3823 and image 3898. This is where the particle movement (e.g. crack) of the 'After' image relative to the 'Before' image is indicated in black. In (D) is the processed frame in PIVlab and above D, the strain rate is in ( $s^{-1}$ ). In red the initial place of the stylolite is indicated, as well as the circumference.

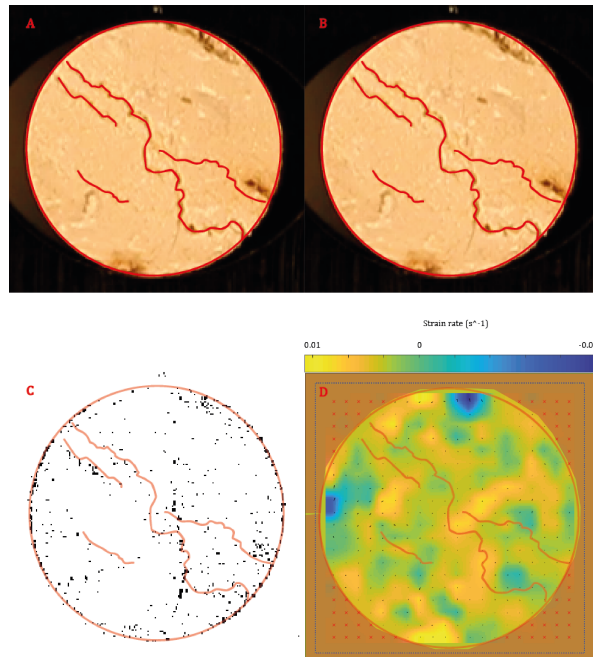


**Figure 6.13: Case 3:** (A) 'Before' Image 4013 is at 80.26 seconds and (B) 'After' Image 4084 is at 81.68 seconds. In (C) is the absolute difference between image 4720 and image 6030. This is where the particle movement (e.g. crack) of the 'After' image relative to the 'Before' image is indicated in black. In (D) is the processed frame in PIVlab and above D, the strain rate is in ( $s^{-1}$ ). In red the initial place of the stylolite is indicated, as well as the circumference.

For TM<sub>313</sub> movie, we mainly encounter Case 1, i.e. random noise (see Table C.1). This happens mainly with a negative  $\Delta Stress/\Delta Disp$ , though also positive  $\Delta Stress/\Delta Disp$ . We encounter Case 2 (i.e. Asymmetric extension) thrice mainly when the  $\Delta Stress/\Delta Disp$  is positive, and Case 3 (i.e. Symmetric extension) only occurs once. Case 3 has a negative  $\Delta Stress/\Delta Disp$ . Also, Case 1 and 2 have the highest  $\Delta Stress$  values.

cases TM <sub>313</sub>				
Region of frames	Case	$\Delta Stress / \Delta Disp$ (Positive or Negative)	$\Delta Stress$ (MPa)	
3106 - 3119	1	Negative	-0.03	
3119 - 3823	1	Positive	+0.88	
3823 - 3898	2	Negative	-2.8	
3898 - 3974	1	Positive	+0.06	
3974 - 3982	1	Negative	-0.03	
3982 - 3991	1	Positive	+0.03	
3991 - 4013	1	Negative	-0.06	
4013 - 4084	3	Negative	-0.03	
4084 - 4196	2	Positive	+0.04	
4196 - 4263	1	Negative	-0.47	
4263 - 4635	2	Positive	+0.16	
4635 - 4172	1	Negative	-0.03	

**Table 6.3:** cases results of TM<sub>241</sub> strain rate in frames. Where  $\Delta Stress / \Delta Disp$  is the stress drop, negative is downwards and positive is upwards. And where MPa is the amount of MPa increase (i.e. positive) or decrease (i.e. negative). Both seen in the stress displacement curve. The cases are described in the introduction of Chapter 6.

As there can be seen in Figure 6.14a the most particle displacement is mainly in the negative  $\Delta Stress / \Delta Disp$ . Furthermore, as there can be seen in Figure 6.14b Case 3 occurs exclusively on the way down, and Case 1 and 2 are more often on the way down, though also on the way up. There is no clear correlation with displacement. Case 2 is observed in the first highest negative  $\Delta Stress / \Delta Disp$  (i.e. after the linear phase of the stress-displacement curve). Case 1 is observed in the second highest negative  $\Delta Stress / \Delta Disp$ .

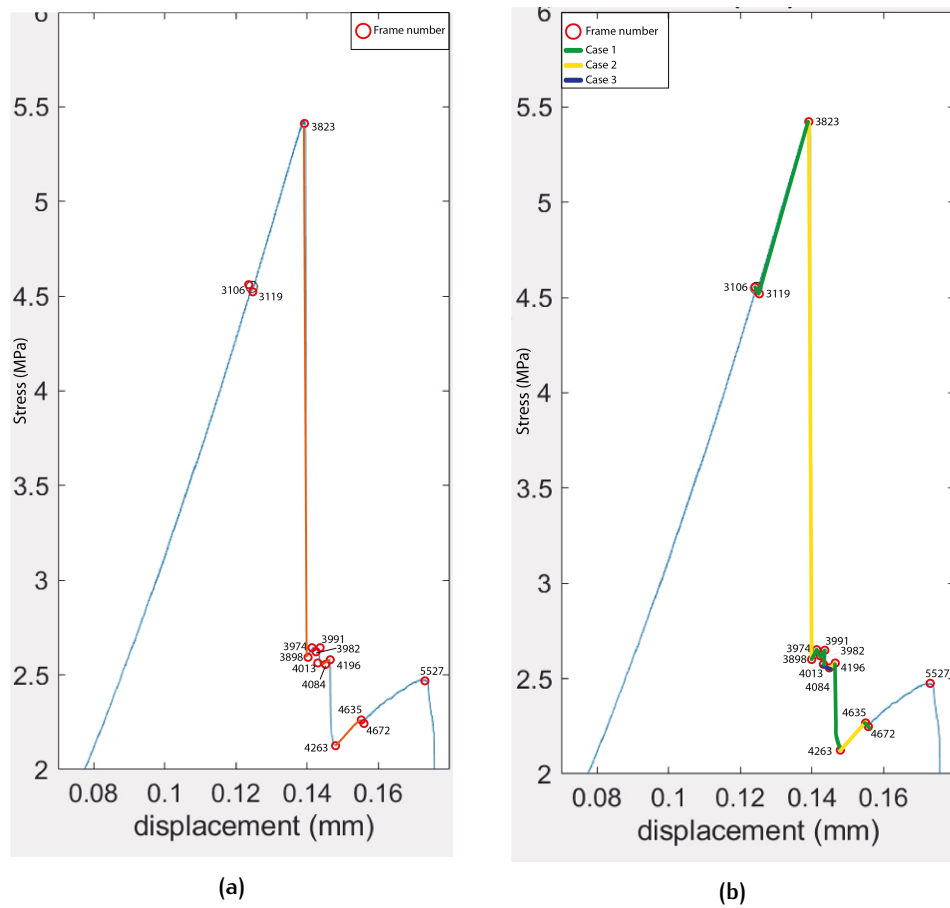


**Figure 6.14:** (a) The red circles are the frame numbers extracted in the peaks and the troughs and the orange lines are the parts where the most activity takes place. (b) The green lines indicate Case 1, the yellow lines indicate Case 2 and the blue lines indicate Case 3.

# 7

## DISCUSSION

### 7.1 LIMITATION OF PIV-METHOD

At first, we attempted to process scenario a) every 10 frames and b) every 50 frames with PIVlab. However, this resulted in a lot of random noise and distinction could not be made anymore (see Figure 6.1 and Figure 6.2 respectively). The noise is a result of too little displacement within each framepair. It can be seen that the velocity vectors are already more clearly for every 50 frames than for every 10 frames. This means that PIVlab is detecting more displacement in 50 frames than in 10 frames but still not enough to give clear results. Every 10 frames uses a time step between consecutive images of 0.2 sec, this is a too small time step to observe obvious results when relating to the stress-displacement curve. When using 50 frames the time step is 1 sec which results in more displacement in the stress-displacement curve between the 'before' image and the 'after' image. This resulted in using the peaks and the troughs of the stress-displacement curve where we were sure that displacement took place.

Also, in this study we used in PIVlab three passes with interrogation areas of 64 pixels gradually decreasing to 32 pixels and ending with small interrogation areas of 16 pixels. However, Thielicke and Stamhuis [2014] stated that if extremely small interrogation areas are used in the last pass the resolution of the vector map will increase but it will also significantly increase noise and the amount of erroneous correlations. In many cases, high vector map resolutions are not really important. Therefore, we choose for a first pass of 64 pixels and for the last pass 16 pixels. However, Thielicke and Stamhuis [2014] suggested to make the first interrogation area as large as possible because it will give more accurate and more reliable results. This could be done in a next study using a first pass of 128 pixels. Using a first pass of 128 pixels gradually decreasing and ending with 16 or 8 pixels pass. This will result in a higher vector map with which PIVlab will obtain more displacement and therefore the results will be more reliable.

Furthermore, in PIVlab the diameter of 29.5 mm of the sample discs was entered by selecting a known reference distance because in PIVlab this is needed to determine how many pixels are one meter. The precision of this kind of calibration is pretty low, so we advice to use external calibration images for the next time the PIV method is used in rock deformation experiments [Thielicke and Stamhuis, 2014].

It is important to note that the 2-D representation in plane strain of PIVlab is not the same as what the 3-D disc specimen will be representing in third dimension [Chen et al., 2020]. Any comparison with experiments is limited by the fact that the BDT sample has many grains supporting the width of the specimen. However, the consequence is likely to be that the heterogeneity on

the level of grain size is enlarged in the 2-D plane strain model [Chen et al., 2020]. The defects in the 2-D model, such as big pores and local areas with fossils is expected to have a larger influence on the stress distribution and concentration, and furthermore the loading history [Chen et al., 2020]. The fracture path can be expected to be more tortuous in these 2-D plane strain model than their 3-D reality [Chen et al., 2020]. The rock property such as strain rate might be overestimated to match the 2-D PIVlab results with the experimental results of the BDT. All these effects reduce the accuracy Chen et al. [2020] of the plane strain rate microstructure model. Since we show that in 2-D the stylolite exerts a strong effect on the location of the fracture, it is expected that stylolites will have an even more critical influence on the meso- or macroscale response of the rock in 3-D.

## 7.2 EXPLANATION RESULTS

The possibility to explain these results is limited by the small number of movies analyzed but what we can say is described here.

In the stress-displacement curves the frame numbers were extracted by visually investigating them from a movie made in preceding study (Pluymakers et al., pers. comm.). To obtain the frame numbers the movie was paused at places where the peaks and the troughs occurred in the stress-displacement curve. This may have led to 'human errors' in pausing the movie at the frame needed. This may have resulted in less accurate results for the frame numbers.

The strain rate is the highest between where the crack initiates and the stylolite on the left side, between the crack and the stylolite the material particles stretch the most and therefore have a positive strain rate. This is what is expected because stylolites most likely weaken the rock due to high porosity and permeability in and around the stylolite region [Baud et al., 2016].

Also, the primary and the secondary fracture follow the curvature of the stylolite. Intuitively a rock is weaker where it bends and therefore it shows this is in line with what was expected.

As there can be seen in Figure 6.6a and 6.10a, the most displacement takes place in the positive  $\Delta Stress / \Delta Disp$  (i.e. upward motion). A reason for this is that the amount of stress is building up. A reason for this is a result of expansion of pre-existing micro-fissures where a cracking effect is generated [Gao et al., 2018]. This should be in Case 3 where there was symmetric extension throughout the sample. This is somewhat contradictory because mostly the highest displacement takes place in the highest negative stress drops ( $\Delta Stress$ ). For example at a point where stress drops rapidly in the stress-displacement curve occurs a fracture [Goodyear and Aspden, 2012]. This should be in Case 2 where there occurred asymmetric extension (i.e. extension between the stylolite and the crack) More research is needed to comprehend this phenomena.

## 7.3 WIDER PERSPECTIVE OF THE STUDY INTO THE FIELD OF APPLIED EARTH SCIENCES

### 7.3.1 Societal relevance

This thesis could be helpful for the geothermal energy sector in the south German Molasse Basin or for the Dinantian carbonates formation in the Netherlands. Both the formations are at approximately 4 km depth. The Geo-temperatures in-situ are dependent on the Geothermal gradient  $G_t$  and in that relation the rock type and the burial history [Wolf, 2020].

$$G_t = \frac{T_f - T_s}{D} \quad (7.1)$$

Where  $G_t$  is the geothermal gradient in [ $^{\circ}\text{C}/\text{km}$ ],  $T_f$  is formation temperature in [ $^{\circ}\text{C}$ ],  $T_s$  is surface temperature in [ $^{\circ}\text{C}$ ] and  $D$  is depth in [km].

In top Dinantian they found in Carlson [2019] that the geothermal gradient could be estimated around 41  $^{\circ}\text{C}/\text{km}$ . In the Molasse Basin the formation temperature could go up to an estimated temperature of 200  $^{\circ}\text{C}$  which means the geothermal gradient of the Molasse Basin can go up to 47.5  $^{\circ}\text{C}/\text{km}$ . However, the temperatures of both formations are mainly estimated between 110 and 160  $^{\circ}\text{C}$ . These temperatures are perfect for Geothermal energy and with the depth of 4 km it is called UDG. UDG energy could potentially make a substantial contribution to the transition towards a sustainable heat supply [Carlson, 2019].

### 7.3.2 Scientific relevance

In general rocks consists of mineral, with pore space that can be filled with fluids (e.g. water) or gases. In all considerations of the composition of rocks, it is essential to keep in mind the effects of scale. This is particularly important with regard to heterogeneity and anisotropy. Rock material viewed at one scale might be homogeneous and isotropic, but viewed at larger or smaller scales it can be neither homogeneous nor isotropic [Wolf, 2020].

For UDG hot water needs to be extracted from the openings (i.e. pores). However, the pores and fractures are not uniformly distributed throughout the rock. Both can be distributed homo- and heterogeneously. Open fractures from the nano-meter to micro-meter scale are widely known to affect the physical properties of rocks, such as compressibility, strength, elastic wave velocities and permeability [Ougier-Simonin et al., 2016]. Fractures can also be seen as elongated pores.

Stylolites are therefore important, because in this study it is concluded that the orientation of stylolites can affect the crack propagation and the behaviour in the two major negative  $\Delta\text{Stress}/\Delta\text{Disp}$  drops in a rock formation, which can therefore influence the permeability or porosity in the formation. Rock properties, including elastic modulus and tensile strength etc., are extensively used for the meso-scale or macro-scale analysis of deformation and occurrence of fractures which usually doesn't include the complexity

of microstructure [Chen et al., 2020]. This study analyzed rock samples at meso-scale (2.95 cm) however because the stylolites (i.e. microstructure) observed in this study have a few mm width the approach is at micro-scale. However at larger scales, such as meso- and macro-scale, formations could be cut by discontinuities like fractures (joints) and divisions between layers. This study could be used as a complementary element to seismic investigation which investigates formations at macro scale. Also, this study indicates the importance of small-scale features, invisible on seismic investigation, on the orientation of the stylolites.

Furthermore, Baud et al. [2016] state that stylolites of  $> 5\text{mm}$  are needed before they affect compressive strength. These stylolites in this study are thinner, and affect tensile strength and fracture orientation significantly.

### 7.3.3 Environmental relevance

Having hot water targets at a depth of 4 km has both advantages and disadvantages: the depth provides the heat, but burial causes compaction, diagenesis and a related decrease in porosity and permeability, making it more difficult for water to flow through the rocks [Bouroullec et al., 2019]. In Baud et al. [2016] they found that samples with a stylolite, independent of the orientation, to be more porous than a stylolite-free rock. However in this study the orientation of the stylolite does affect the tensile strength and fracture orientation. To enhance the permeability of the formation hydraulic fracturing (i.e. increase the opening of the cracks in the formation) may be an option for UDG energy.

In the south and the west of the Netherlands the Mesozoic extensional basins has a NW-SE orientation [de Jager, 2007]. Hydraulic fracturing may enhance the porosity and permeability and consequently increase the water flow in a reservoir throughout a rock formation. Reservoirs are very heterogeneous due to the complex sedimentary processes and post-sedimentary events. The spatial distribution of heterogeneities, which appear on various length scales, may significantly influence the flow behavior and consequently the reservoir performance [Masihi et al., 2016]. On micro-scale heterogeneities (e.g. stylolites) can play a role in the flow behavior of water.

However, using hydraulic fracturing with a basin which is NW-SE oriented it is important to note that the stylolite changes how the hydrofractures should be oriented to enhance the permeability. Despite the impact that hydraulic fracturing has had on the energy sector, the physical mechanisms that control its efficiency and environmental impacts remain poorly understood in part because the length scales involved range from nanometres (i.e. micro-scale) to kilometres (i.e. macro-scale) [Hyman et al., 2016]. This study can be helpful for obtaining knowledge about how hydraulic fracturing at micro-scale impacts rock formations (e.g. TM and Dinantien formation).

#### 7.3.4 BSc-curriculum

The following courses of the curriculum of BSc-Applied Earth Sciences were important to conduct this study:

- Matlab and Systems
- Geophysical Methods for Subsurface Characterization
- Sedimentology
- Extraction of Resources
- Petrophysics and Image Analysis
- Flow through Porous Media

In order to begin with this study a sufficient knowledge of material such as rocks and in particular carbonates was needed. Stylolites were already mentioned in the Sedimentology course, so a rough idea of this kind of heterogeneity was already known.

Furthermore, to use the PIVlab software, a understanding of programming was needed, in particular Particle Image Velocimetry. A huge part of this study was data processing with Software and MATLAB (see D. To use a particular Software such as PIVlab, knowledge was needed from the course of Petrophysics and Image Analysis, where data was extracted from experiments and used to describe behaviour/influence of rocks on permeability or porosity.

Also, the types of experimental tests should be known in the field of geo-sciences. Also common material behaviour when tested in a laboratory should be familiar. The experimental methods were deeply described in the Extraction of Resources course where it was needed to describe the data in a quantitative and qualitative way. Here the stress-strain relationship was needed to understand, and in particular stress-displacement curves. Furthermore, mechanical properties such as elastic properties and the inelastic properties an in-depth knowledge was obtained from the Petrophysics and Image Analysis course and applied in this study. The stress-strain curves have identical behaviour for rocks such as a linear elastic region in the beginning. Furthermore the strength of a rock determined the failure and the fractures of a rock.

To answer the question on what this study means for in the field of Applied Earth Sciences and a wider engineering perspective it was necessary to zoom out. In particular for a sustainable heat energy source such as geothermal energy. The material studied was from a Geothermal Basin in southern Germany, and the theory behind geothermal energy is dependent on flow through porous media. In the course Flow through Porous media, knowledge was obtained from how water flows through a surface and what the influence on reservoirs or lakes in the neighbourhood is on the an aquifer well.

## 7.4 RECOMMENDATION

In this study, the motion of tensional failure is only investigated for 3 samples. However, in the future this should be expanded to eleven. Now, one sample with a oblique stylolites of  $40^\circ$  and two samples with vertical stylolites of  $90^\circ$  are investigated. To give a better and more reliable conclusion about the influence of the orientation of the stylolites on the strain rate and crack propagation and consequently on the permeability, more samples should be processed in PIVlab and analysed as in this thesis.

Furthermore, experiments are carried out in 3-D and we used a 2-D model on that data. A more detailed study is reserved for future authors who can use 3-D loading and 3-D models instead of a 2-D model such as PIVlab. In situ stress states are basically three-dimensional (3-D), and therefore it is important to develop 3-D models for this purpose.

# 8

## CONCLUSION

By performing Particle Image Velocimetry (PIV) and image analysis on three different samples, all including a stylolite we identified three common cases. The definitions of the three common cases are:

1. Random extension and compression: positive and negative strain rate are randomly distributed in the sample.
2. Asymmetric extension: positive strain rate occurs in between stylolite and crack.
3. Symmetric extension: positive strain rate occurs around stylolite.

After identifying the three common cases (Case 1, Case 2 and Case 3), we correlate their occurrence with their location on the stress-displacement curves to obtain information about the cases in the stress drops (i.e.  $\Delta Stress / \Delta Displacement$ ), where positive is on the way up and negative is on the way down in the stress-displacement curve.

In this study we found the following:

- In the samples with stylolites, always more than one fracture was formed. A primary fracture and a secondary fracture.
- The positive strain rate is the highest in between the stylolite and/or the primary and secondary fracture.
- The primary and the secondary fracture follow the curvature of the stylolite.
- For the two  $90^\circ$  oriented stylolites we mainly encountered Case 1 in negative stress drops.
- For the two  $90^\circ$  oriented stylolites we encountered Case 2 only in positive stress drops.
- For the two  $90^\circ$  oriented stylolites the most particle displacement takes place in the positive stress drops.
- For the two  $90^\circ$  oriented stylolites Case 1 takes place at the first highest negative stress drop from the stress-displacement curve.
- For the two  $90^\circ$  oriented stylolites Case 3 takes place at the second highest negative stress drop from the stress-displacement curve.
- For the  $40^\circ$  we encountered Case 1 both in negative and positive stress drops.

- For the  $40^\circ$  oriented stylolite we encountered Case 2 thrice mainly when the stress drop is positive.
- For the  $40^\circ$  oriented stylolite the most particle displacement is mainly in the negative stress drop.
- For a  $40^\circ$  oriented stylolites Case 2 takes place at the first highest negative stress drop from the stress-displacement curve.
- For the  $40^\circ$  oriented stylolites Case 1 takes place at the second highest negative stress drop from the stress-displacement curve.
- The orientation of a stylolite in a sample influence the stress-displacement curve in such a way that Case 1, 2 and 3 does not take place at the same stress drops.
- All 3 have a unique strain rate per stress drop pattern.

## BIBLIOGRAPHY

- Alsharhan, A. and Sadd, J. (2000). Stylolites in lower cretaceous carbonate reservoirs. *SEPM Spec. Publ.* 69, 69:185–207.
- Baud, P., Rolland, A., Heap, M. J., Xu, T., Nicolé, M., Ferrand, T., Reuschlé, T., Toussaint, R., and Conil, N. (2016). Impact of stylolites on the mechanical strength of limestone. *Tectonophysics*.
- Bouroullec, R., Nelskamp, S., Kloppenburg, A., Fattah, A. R., Foeken, J., ten Veen, J., Geel, K., Debacker, T., and Smit, J. (2019). Burial and structural analysis of the dinantian carbonates in the dutch subsurface. [Online; accessed 10-June-2020].
- Bruna, P.-O., Lavenu, A., Matonti, C., and Bertotti, G. (2019). Are stylolites fluid-flow efficient features? *Journal of Structural Geology*, 125:270–277.
- Carlson, T. (2019). Petrophysical report of the dinantian carbonates in the dutch subsurface: facies analysis and diagenetic evolution of the dinantian carbonates in the dutch subsurface. [Online; accessed 03-June-2020].
- Chen, B., Xiang, J., Latham, J.-P., and Bakker, R. R. (2020). Grain-scale failure mechanism of porous sandstone: An experimental and numerical fdem study of the brazilian tensile strength test using ct-scan microstructure. *International Journal of Rock Mechanics and Mining Sciences*, 132:104348.
- de Jager, J. (2007). Geological development. *Geology of the Netherlands*, pages 5–26.
- Gao, F., Cai, C., and Yang, Y. (2018). Experimental research on rock fracture failure characteristics under liquid nitrogen cooling conditions. *Results in Physics*, 9.
- Goodyear, S. and Aspden, R. (2012). Mechanical properties of bone ex vivo. *Methods in molecular biology (Clifton, N.J.)*, 816:555–71.
- Hendrich, M. M. . A. (2002). Deutsche stratigraphische kommission. [Online; accessed 10-June-2020].
- Humphrey, E., Gomez-Rivas, E., Koehn, D., Bons, P., Neilson, J., Martín-Martín, J. D., and Schoenherr, J. (2019). Stylolite-controlled diagenesis of a mudstone carbonate reservoir: A case study from the zechstein 2 carbonate (central european basin, nw germany). *Marine and Petroleum Geology*, 109.
- Hyman, J., Jimenez-Martinez, J., Viswanathan, H., Carey, B., Porter, M., Rougier, E., Karra, S., Kang, Q., Frash, L., Chen, L., Lei, Z., O'Malley, D., and Makedonska, N. (2016). Understanding hydraulic fracturing: A multi-scale problem. *Philosophical Transactions of The Royal Society A Mathematical Physical and Engineering Sciences*, 374:20150426.

- Klapperich, H. (2014). Environmental geotechnics energies – “energiewende” in germany = deep geothermal energy =. *Geosciences and Engineering*, 3:13–23.
- Li, D. and Wong, L. (2012). The brazilian disc test for rock mechanics applications: Review and new insights. *Rock Mechanics and Rock Engineering*, 46.
- López-Buendía, A., Guillem, C., Cuevas, J., Mateos, F., and Montoto, M. (2013). Natural stone reinforcement of discontinuities with resin for industrial processing. *Engineering Geology*, 166:39 – 51.
- Masihi, M., Gago, P. A., and King, P. R. (2016). Estimation of the effective permeability of heterogeneous porous media by using percolation concepts. *Transport in Porous Media*, 114:169–199.
- Ougier-Simonin, A., Renard, F., Boehm, C., and Vidal-Gilbert, S. (2016). Microfracturing and microporosity in shales. *Earth-Science Reviews*, 162:198–226.
- Peng, S. and Zhang, J. (2007). *Rock properties and mechanical behaviors*, pages 1–26. Springer Berlin Heidelberg, Berlin, Heidelberg.
- Tamáskovics, N., Tondera, D., Blöcher, G., Moeck, I. S., Pavlov, P., Bems, C., and Hild, S. (2014). Geothermal research project “algäu 2.0” research concepts, laboratory investigations and planning operations.
- Thielicke, W. and Stamhuis, E. J. (2014). Pivlab – towards user-friendly, affordable and accurate digital particle image velocimetry in matlab. *Journal of Open Research Software*, 2.
- Toussaint, R., Aharonov, E., Koehn, D., Gratier, J.-P., Ebner, M., Baud, P., Rolland, A., and Renard”, F. (2018). Stylolites: A review. *Journal of Structural Geology*, 114:163 – 195.
- Wikipedia (2020). BMP file format — Wikipedia, the free encyclopedia. [Online; accessed 08-May-2020].
- Wolf, K. H. (2020). Introduction to the physics of rocks: theory and applications.
- Xu, J.-m., Cheng, C.-h., and Lu, H.-p. (2011). Strain field investigation of limestone specimen under uniaxial compression loads using particle image velocimetry. *Journal of Central South University of Technology*, 18:1619–1625.

# A

TM236

In this chapter the remaining figures are displayed for movie TM236. Also a table which is used for analyzing the figures is given. In here the three common cases of results can be observed.

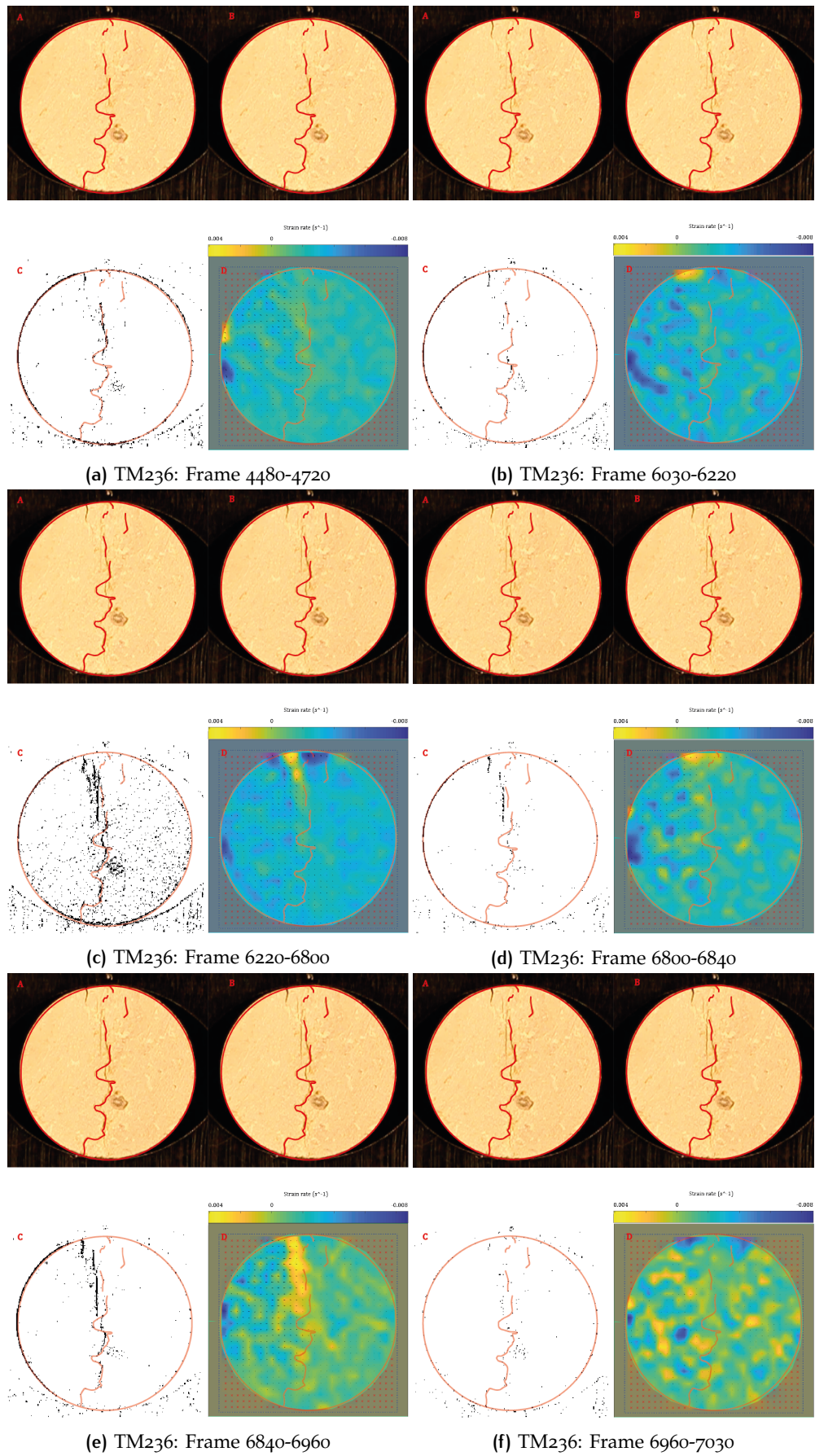
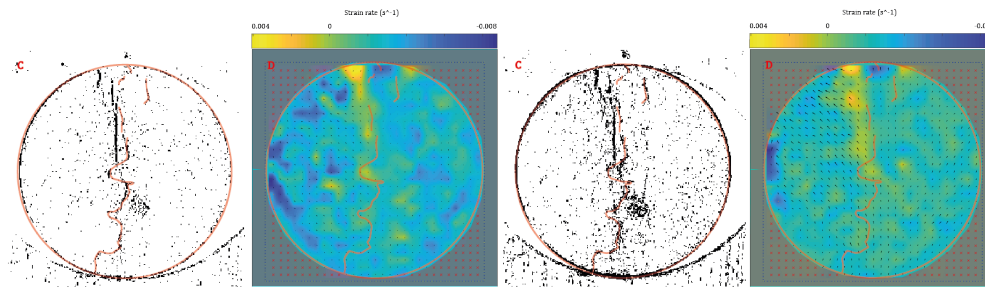
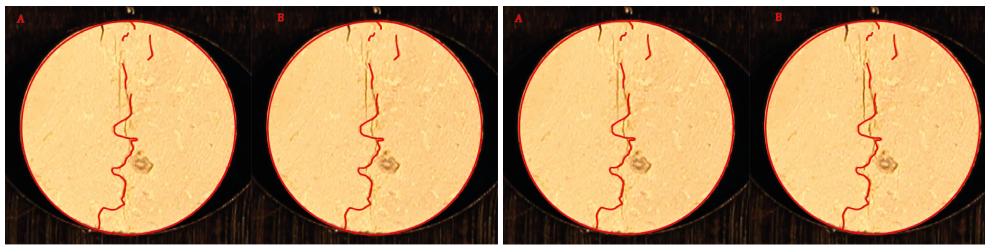
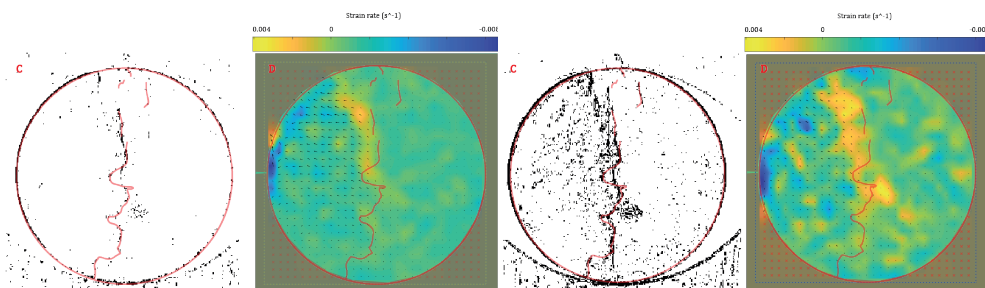
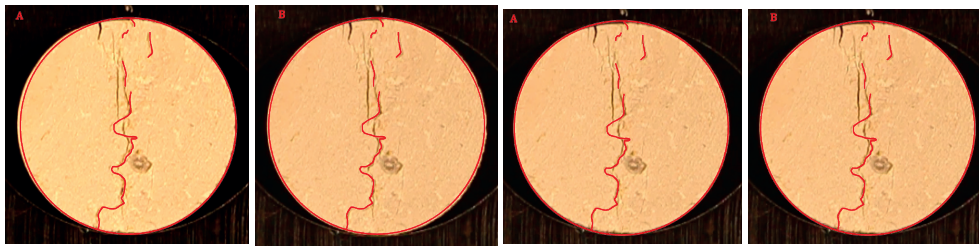


Figure A.1: TM236 Frames



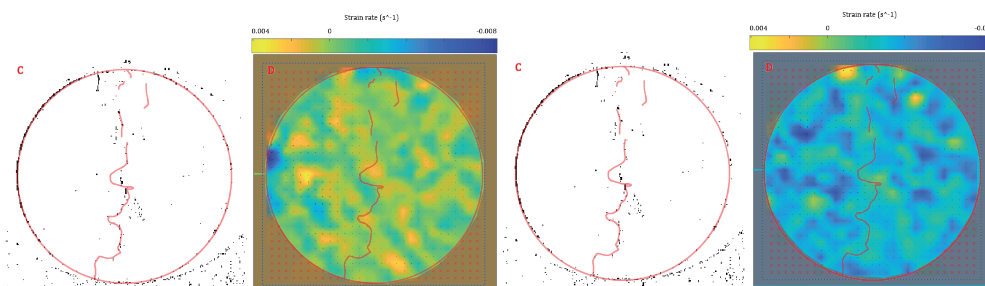
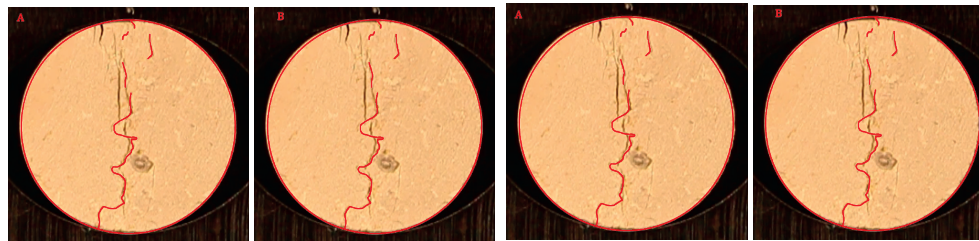
(a) TM236: Frame 7030-7640

(b) TM236: Frame 7640-9430



(c) TM236: Frame 9430-10019

(d) TM236: Frame 10019-10389



(e) TM236: Frame 10389-10535

(f) TM236: Frame 10535-10737

Figure A.2: TM236 Frames

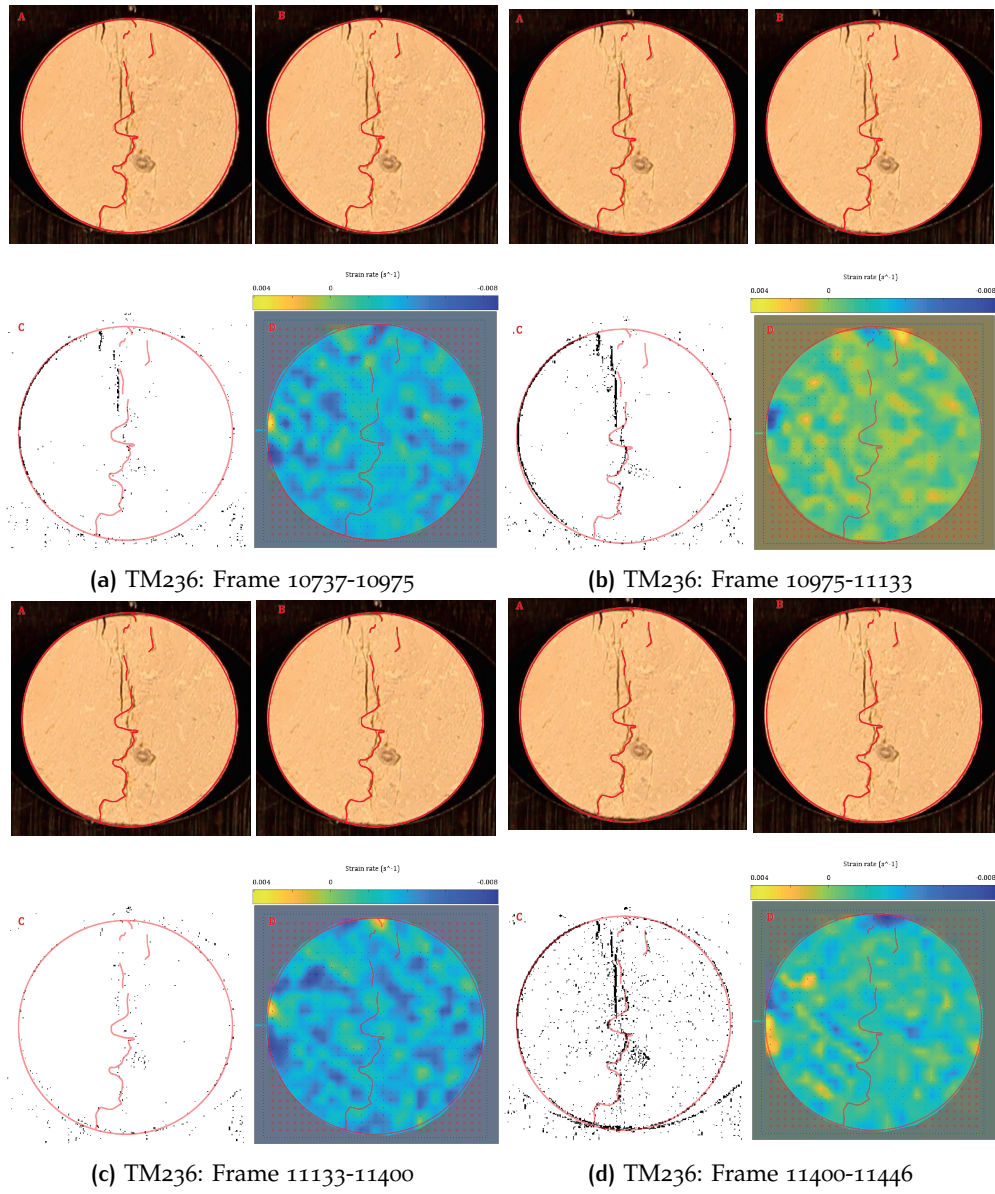


Figure A.3: TM236 Frames

Observations TM236			
Region of frames	Comment on strain rate	Notes	Case
4180 - 4280	More positive strain rate on the left side of the stylolite	Random distributed throughout sample	1
4280 - 4480	Highest positive strain rate in between the stylolite at the top and the stylolite which propagates a little lower	Initiate of micro-cracks around stylolite and top of sample	3
4480 - 4720	Strain rate centered around the stylolite	Crack propagation	1
4720 - 6030	Highest positive strain rate centered around the stylolite	First crack propagates throughout the whole stylolite region	2
6030 - 6220	Highest positive strain rate on the left side of the stylolite where the crack propagates	Random distributed throughout sample	1
6220 - 6800	Highest positive strain rate in between the stylolite at the top and the stylolite which propagates a little lower	Crack propagation at top	2
6800 - 6840	Highest positive strain rate in between the stylolite at the top and the stylolite which propagates a little lower	Crack propagation at top	1
6840 - 6960	Highest positive strain rate centered around the stylolite	Crack propagates throughout the whole stylolite region	2
6960 - 7030	Positive and negative strain rate	Random distributed throughout sample	1
7030 - 7640	Highest positive strain rate in between the stylolite at the top and the stylolite which propagates a little lower	Crack propagation	2
7640 - 9430	Highest positive strain rate in between the stylolite at the top and the stylolite which propagates a little lower	Rock breaks and crack propagation to the left	2
9430 - 10019	Highest positive strain rate in between the stylolite at the top and the stylolite which propagates a little lower	Crack propagation to the left	2
10019 - 10389	Highest positive strain rate in between the stylolite at the top and the stylolite which propagates a little lower	Initiate of micro-cracks around stylolite and top of sample	3

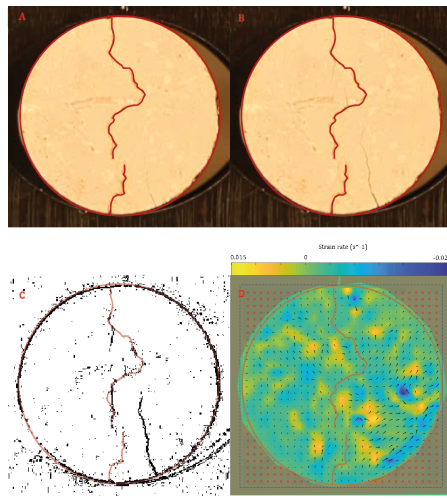
Table A.1: Observations of TM236 strain rate in frame 4180 until 10389

Observations TM236				
Region of frames		Comment on strain rate	Notes	Case
10389 10535	-	Positive and negative strain rate	Random distributed throughout sample	1
10535 10737	-	Positive and negative strain rate	Random distributed throughout sample	1
10737 10975	-	Positive and negative strain rate	Random distributed throughout sample	1
10975 11133	-	Positive and negative strain rate	Random distributed throughout sample	1
11133 11400	-	Positive and negative strain rate	Random distributed throughout sample	1
11400 11446	-	Positive and negative strain rate	Random distributed throughout sample	1
11446 12770	-	Positive and negative strain rate	Random distributed throughout sample	1

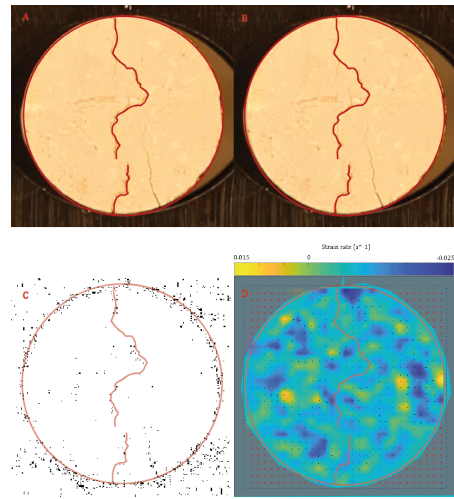
Table A.2: Observations of TM236 strain rate in frame 10389 until 12770

# B | TM241

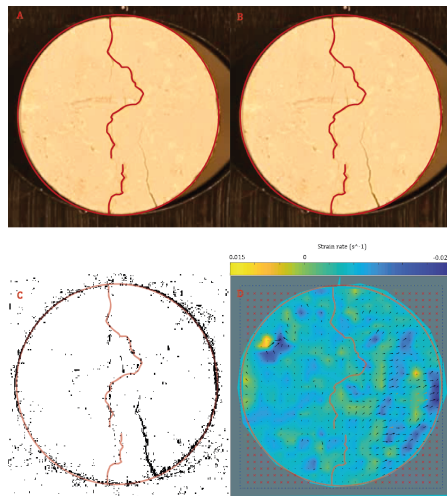
In this chapter the remaining figures are displayed for movie TM241. Also a table which is used for analyzing the figures is given. In here the three common cases of results can be observed.



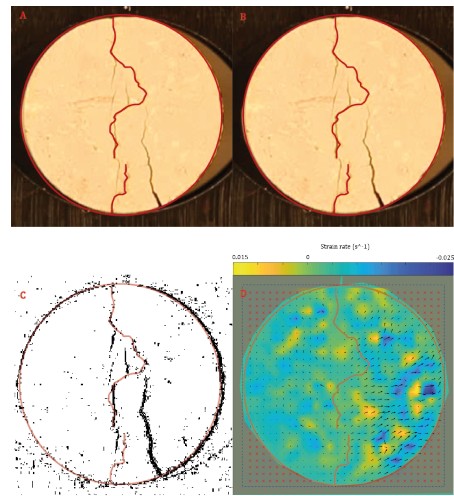
(a) TM241: Frame 3084-4303



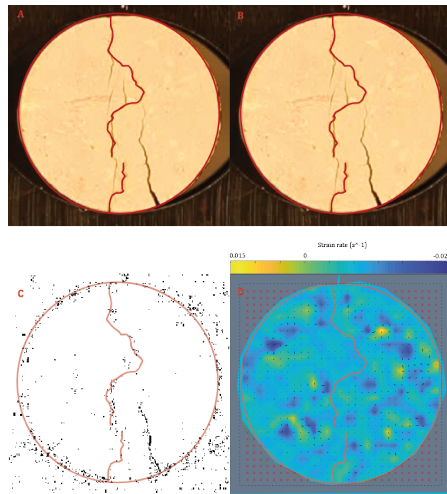
(b) TM236: Frame 4304-4359



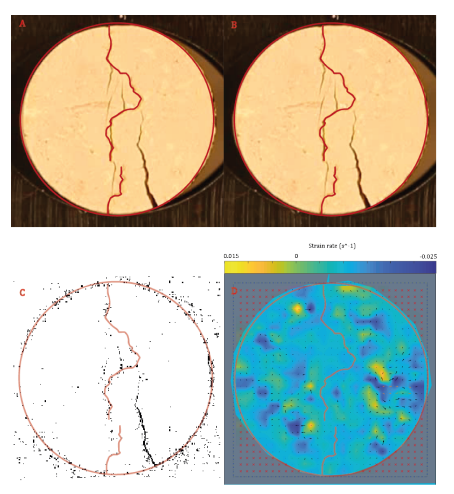
(c) TM236: Frame 4359-4859



(d) TM236: Frame 5136-5801



(e) TM236: Frame 5801-5857



(f) TM236: Frame 6079-6190

Figure B.1: TM241 Frames

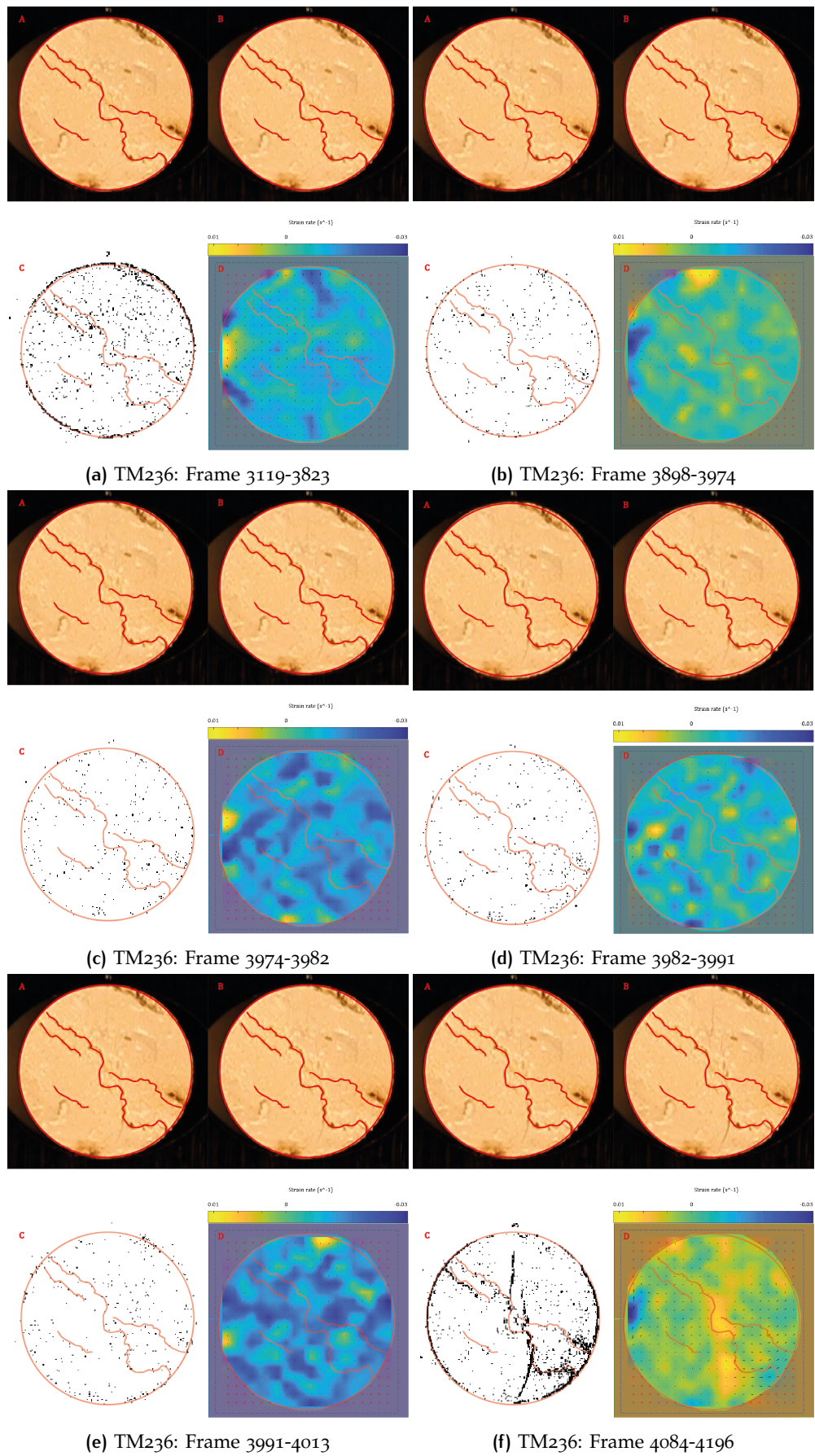
Observations TM241			
Region of frames	Comment on strain rate	Notes	Case
2900 - 3084	More positive strain rate on the right bottom side of the stylolite	Random distributed throughout sample	1
3084 - 4304	Highest positive strain rate in between the stylolite and the stylolite at the bottom and the crack	First cracks	3
4304 - 4359	Not a lot of strain rate, more negative than positive	Random distributed throughout sample	1
4359 - 4859	Highest positive strain rate centered around the stylolite and in between the crack and the stylolite	Crack propagation	1
4859 - 5136	Highest positive strain rate on the right corner side of the stylolite where the crack propagates	Rock breaks	3
5136 - 5801	Highest positive strain rate centered around the stylolite and in between the crack and the stylolite	Crack propagation	2
5801 - 5857	Strain rate more negative than positive	Random distributed throughout sample	1
5857 - 6079	Highest positive strain rate on the right corner side of the stylolite and in between where the crack propagates	crack propagates to the right	2
6079 - 6190	More negative strain rate around stylolite, highest strain rate to the right of the crack	Random distributed throughout sample	1

Table B.1: Observations of TM241 strain rate in frames



# C | TM313

In this chapter the remaining figures are displayed for movie TM<sub>313</sub>. Also a table which is used for analyzing the figures is given. In here the three common cases of results can be observed.

Figure C.1: TM<sub>313</sub> Frames

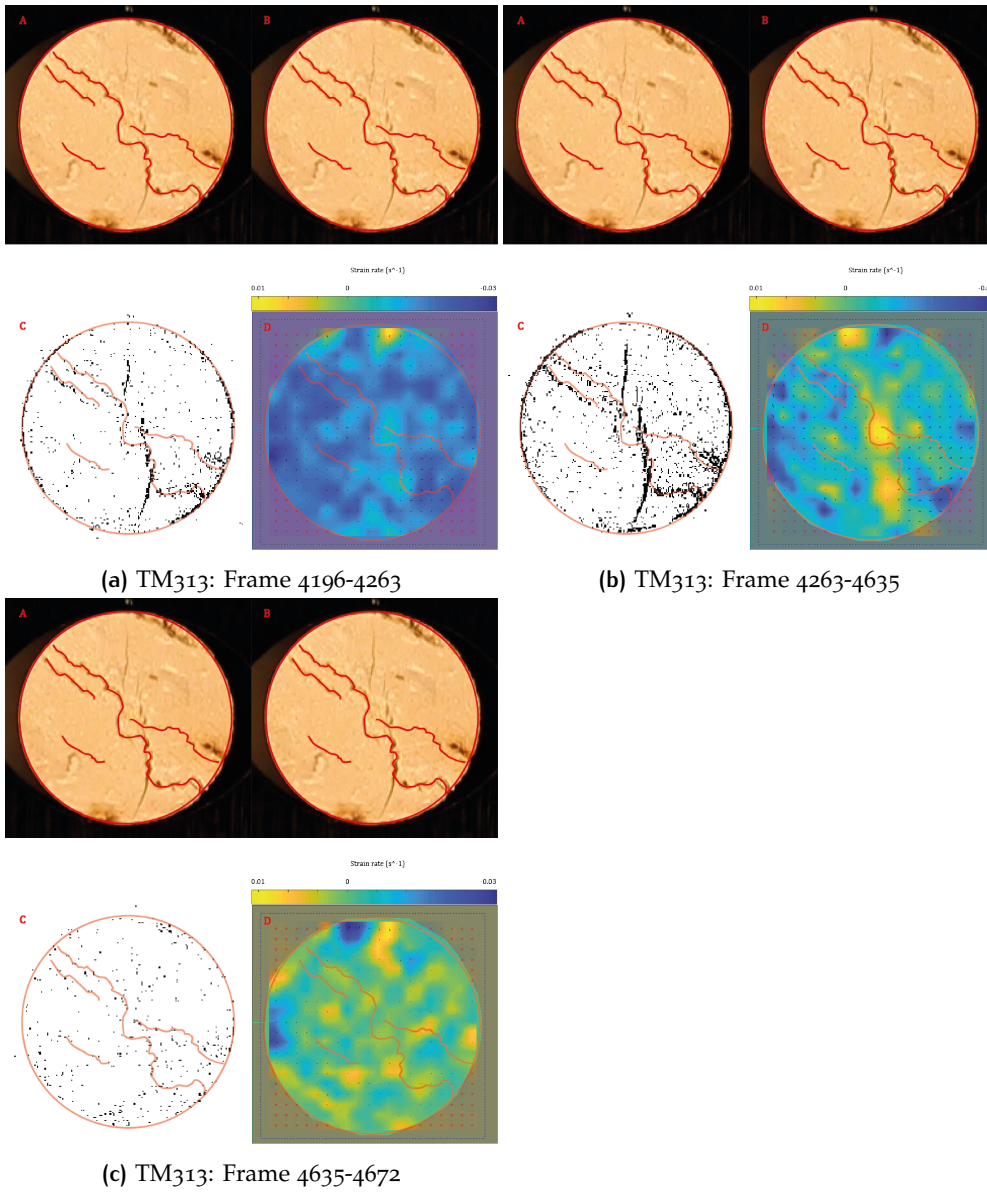


Figure C.2: TM313 Frames

Observations TM313				
Region of frames	Comment on strain rate	Notes	Case	
3106 - 3119	Same amount of positive and negative strain rate throughout sample	Random distributed throughout sample, initiation of micro-cracks	1	
3119 - 3823	On the left side of the sample high positive strain rate can be observed and negative strain rate in the vertical oriented in the middle of the sample	Random distributed throughout sample, initiation of micro-cracks	1	
3823 - 3898	Highest positive strain rate centered around the stylolites	Crack propagates throughout the stylolite region	2	
3898 - 3974	Same amount of positive and negative strain rate throughout sample	Random distributed throughout sample, initiation of micro-cracks	1	
3974 - 3982	Highest negative strain rate throughout sample	Random distributed throughout sample	1	
3982 - 3991	Same amount of positive and negative strain rate throughout sample	Random distributed throughout sample, initiation of micro-cracks	1	
3991 - 4013	Highest negative strain rate throughout sample	Random distributed throughout sample	1	
4013 - 4084	Highest positive strain rate centered throughout sample	Crack propagates throughout the stylolites region	3	
4084 - 4196	Highest positive strain rate centered around the stylolites	Rock breaks	2	
4196 - 4263	Highest negative strain rate throughout sample	Random distributed throughout sample	1	
4263 - 4635	Highest positive strain rate centered throughout sample	Crack propagates in the bending of the stylolites region	2	
4635 - 4672	Same amount of positive and negative strain rate throughout sample	Random distributed throughout sample	1	

Table C.1: Observations of TM236 strain rate in frames

# D | TIMETABLE

Table D.1: Subjects Timetable

**Tijdschrijfformulier BSc eindwerk**

<b>onderdelen</b>
weekly skype meeting (wk1 - wk10)
<i>voorstudie fase</i>
startbijeenkomst with Dr. Wolf (wk1)
informatie inwinnen (Google scholar, Researchgate, ScienceDirect, Scopus etc.) (wk1-wk4)
overleg met derden
assistentie bij begeleider (wk1-wk10)
Introductie schrijven (wk2)
<i>conceptvorming/modelvorming/ (wk2-wk5)</i>
methode schrijven
resultaten krijgen en beschrijven met Matlab en Toolbox
<i>analyse (wk5-wk7)</i>
analyseren resultaten en literatuur bekijken (wk5-wk6)
conclusies aan resultaten verbinden? (wk6-wk7)
schrijven tussenrapport + process feedback (wk6- wk9)
presentatie tussenrapport (wk7)
<i>Uitwerking (wk7-wk9)</i>
schrijven eindrapport (zie ook tussenrapport) + process feedback (wk8-wk9) conclusie schrijven (wk-8) samenvatting schrijven en final details (wk-9)
check door derden op spelling etc. (wk-9)
printen en binden (wk9)
voorbereiden presentatie (wk10)
presentatie maken en oefenen (wk10)
evaluatie met begeleider (wk10)









Table D.6: Week 8 - Week 9

wk 8 (8-6 - 14-6) (Process feedback + Deadline draft + Deadline monitor report)	wk 9 (15-6 - 21-6) (Deadline extra chapter)
12-6 09:00 - 10:00 (1)	
9-6 13:45-15:00 (1.25)	
8-6 09:00 - 17:00 (8) + Send draft report to supervisor 9-6 09:00 - 13:45 (4.75) 15:00 - 17:00 (2) 10-6 08:00 - 16:00 (8) 11-6 08:00 - 16:30 (8.5) 12-6 10:00 - 17:00 (7)	
12-6 08:00 - 09:00 (1)	
	15-6 09:00 - 17:00 (8) 16-6 07:45 - 16:45 (9) 17-6 08:45 - 16:45 (8) 18-6 08:00 17:00 (9) 19-6 08:00 - 17:00 (9) + Send final draft to supervisor
41.5	43



## COLOPHON

This document was typeset using  $\text{\LaTeX}$ . The document layout was generated using the `arsclassica` package by Lorenzo Pantieri, which is an adaption of the original `classicthesis` package from André Miede.



